Topical Review

# Towards Monolithic Integration of Germanium Light Sources on Silicon Chips

**Shinichi Saito[1], Abdelrahman Zaher Al-Attili[1], Katsuya Oda[2] & Yasuhiko Ishikawa[3]**

[1] Nanoelectronics and Nanotechnology Research Group, Electronics and Computer Science, Zepler Institute, Faculty of Physical Sciences and Engineering, University of Southampton, SO17 1BJ, United Kingdom

[2] Research & Development Group, Hitachi, Ltd., 1-280 Higashi-Koigakubo, Kokubunji, Tokyo 185-8601, Japan

[3] Department of Materials Engineering, Graduate School of Engineering, The University of Tokyo, Tokyo, Japan

E-mail: S.Saito@soton.ac.uk

November 2015

**Abstract.** Germanium (Ge) is a group-IV indirect band gap semiconductor, and therefore bulk Ge cannot emit light efficiently. However, the direct band gap energy is close to the indirect one, and significant engineering efforts are being made to convert Ge into an efficient gain material monolithically integrated on a Si chip. In this article, we will review the engineering challenges of developing Ge light sources fabricated using nano-fabrication technologies compatible with Complementary Metal-Oxide-Semiconductor (CMOS) processes. In particular, we review recent progress in applying high-tensile strain to Ge to reduce the direct band gap. Another important technique is doping Ge with donor impurities to fill the indirect band gap valleys in the conduction band. Realization of carrier confinement structures and suitable optical cavities will be discussed. Finally, we will discuss possible applications of Ge light sources in potential photonics-electronics convergent systems.

PACS numbers: 73.21.-b,73.21.Fg,73.40.Qv,73.63.Hs,78.60.Fi,78.55.-m,78.67.-n,78.67.De,85.60.Jb

*Keywords*: Si photonics, Ge, light source Submitted to: *Semicond. Sci. Technol.*

## 1. Introduction

Feynman precisely predicted the emergence of hand-held mobile computers with human face recognition systems [1] in 1959, when historical patents for Integrated Circuits (ICs) were filed by Kilby [2] and Noyce [3]. Currently, more than 1 billion Complementary-Metal-Oxide-Semiconductor (CMOS) Field-Effect Transistors (FETs) are integrated in a Large-scale IC (LSI), and the semiconductor industry has been continuously scaling down the channel length of FETs in the last 4 decades towards sub-10-nm technology nodes [4, 5]. In addition to the electronic integration, various photonic devices have also been integrated on silicon (Si) [6–17].

Currently, a Laser-Diode (LD) using a group III-V compound semiconductor is used in a commercially available Si photonic chip [6–17]. In this device, the coherent light from the III-V LD propagates through an optical fibre, which is coupled to a Si waveguide (WG) through a grating coupler [18]. Another scheme is to employ a hybrid integration of III-V materials on Si, where a propagating mode in a Si WG is evanescently coupled to an optical gain medium made of a III-V material [19–22]. While the use of III-V materials [15, 17, 19, 22, 23] is a practical option available in the near-term, there are growing needs to develop monolithic light sources compatible with CMOS processes in order to reduce the cost for manufacturing, while ensuring the scalability and high yields [5, 24–31]. Therefore, significant efforts are being made to develop group-IV LDs, however group IV materials like Si and Ge are in-direct band gap semiconductors.

After the discovery of efficient light emission from porous-Si by quantum confinements [32, 33], the performance of Si-based light sources has steadily improved over the years [6, 7, 9, 30, 34–40]. In particular, a quantum efficiency exceeding 23 % was achieved by passivating the surface using high-pressure water vapour annealing [35, 38]. These Si-based light sources would be useful for applications with wide wavelengths over a wide rang of visible to near-infrared (NIR). However, they are not compatible with Si photonic passive devices using a Si WG, since the emitted light from a quantum confined Si nano-structure is blue-shifted compared with the band gap energy of Si (1.1 eV), and thus it will be strongly absorbed in a Si WG.

Germanium (Ge) is an another promising material compatible with CMOS processes; the band gap of Ge is around 0.8-eV [41, 42], corresponding to a wavelength of 1550 nm, which is commonly used in glass fibres due to the minimum in absorption losses at this wavelength. Ge has already been introduced in CMOS processes for strain-engineering at the source and the drain of $p$-channel MOSFETs [4, 43–45], and Ge is also used for photo-detectors (PDs) in Si photonics [5, 46, 47]. If a practical Ge LD is available, we can realize full monolithic integration of Opto-Electronic Integrated Circuits (OEICs) with Ge LDs, Ge PDs, Si WGs, modulators, and many other optically passive components like splitters and gratings [6–16]. Currently, there are several reports on successful laser operation of Ge Fabry-Perot (FP) WGs by optical pumping [48] and by electrical pumping [49–51] at room temperature, in addition to Terahertz (THz) lasers in Ge at low temperatures [52–54]. The recent success on germanium-

tin ($Ge_{1-x}Sn_x$) lasers by optical pumping at low temperatures [55] also proved the theoretical prediction of the direct-indirect transition upon changing the composition, $x$ [56, 57]. There are many review articles [5, 24–31, 58, 59] covering recent progress on the development of Ge-based light sources, which prove significant attention has been directed to this area. In order to avoid duplicating other reviews, our focus in this article is to introduce wide varieties of technological options for enabling direct recombination in Ge. Some pedagogical introductions to light-emission, waveguides, and strain-engineering are summarized in the appendices. We will also raise and discuss many unknown fundamental issues such as requirements for positive optical gain from Ge, which must be addressed by research communities for the future.

## 2. Various technological approaches for Ge-based light sources

In this section, we will overview various technical approaches to develop Ge-based light sources using Si processes, and we will discuss technical details in the later sections. Figure 1 shows a schematic summary of various options to fabricate Ge-based light sources. Of course, there are many other process options, which are not covered in Fig. 1. The conventional wisdom for developing a new LD is to heavily rely only on epitaxial growth techniques [60, 61]. Whilst fully respecting the importance of the process developments in epitaxial growth, however, we feel that other routes towards the development of Ge-based light sources will also be important, since various nano-fabrication technologies are available in Si processes in addition to epitaxial growth. However, the technical hurdle of converting an indirect band gap semiconductor to a direct band gap semiconductor is not easy to overcome, and the use of all available technologies in Si processes should be considered for Ge-based light sources.

The first big choice is material selections to be used for the active gain media and cladding layers. Pure Ge is the most widely used material [5, 25–30, 59] in this area, while there is an increasing number of publications on GeSn as well [31, 55, 58]. In order to grow these materials various deposition process technologies are used such as Ultra-High-Vacuum-Chemical-Vapour-Deposition (UHV-CVD) [24, 46–48, 50, 62–65], Molecular-Beam-Epitaxy (MBE) [51, 66–69], Reduced-Pressure-Chemical-Vapour-Deposition (RP-CVD) [70–74], Low-Energy Plasma-Enhanced-Chemical-Vapour-Deposition (LEPE-CVD) [75–78], and so on.

The next choice is the structure of the active materials. Most of the research activities are based on bulk Ge [5, 25–31, 58, 59]. However, considering the history of III-V LDs, there are significant advantages in reducing the Dimensionality ($D$) [60, 61, 79] from bulk ($3D$) to Quantum-Well (QW, $2D$) [80], Nano-Wire (NW, $1D$) and down to Quantum-Dot (QD, $0D$) architectures to achieve lower threshold currents for laser operation and improve high temperature operation [79]. GeSn [31, 58] is particularly promising in this regard, since the double heterostructures with type-$I$ band alignments are theoretically proposed [81]. Here, we would like to emphasize the possibilities of using patterning techniques such as lithography and etching to make these quantum nano-

structures [30, 82–84]. Currently, dry-etched vertical Si QWs called fins [82, 85] were successfully introduced in mass production as FinFETs for CMOS [4]. The structures like fins, NWs, or QDs, can be patterned using standard Si processes, and top-down pattering technologies will play an important role for the development of Ge-based light sources in addition to conventional epitaxial growth technologies [30].

Other key piece for the fabrication of Ge light sources is $n$-type doping and stress-engineering [5, 25, 26, 28–30, 59], which are certainly different from the III-V LDs technologies. This is coming from the quasi-direct band gap character of Ge, which has a conduction minimum at the $L$ point [28, 59, 86–90], whose energy is about 0.14-eV smaller than the bottom of the conduction band minimum at the $\Gamma$ point. It was proposed by Liu [86] to dope with $n$-type impurities to fill the $L$-valley with carriers, while additional electrons and holes populated by optical or electrical pumping will be efficiently injected to the $\Gamma$ point. Following the proposal, there were many experimental reports confirming the enhanced light emission from Ge by various processes such as *in-situ* doping during growth [24, 63–65], ion implantation [91], Spin-On-Dopant (SOD) [67–69, 92], and so on. There is no consensus on the exact values of how much doping would be required to expect positive optical gain values from Ge [30, 31, 59, 77, 90]. The emergence of positive optical gain also depends on the lifetime of excess carriers [93–97], which is quite sensitive to the quality of Ge. We will further review doping processes in Sec. 5.

Moreover, it was theoretically predicted that Ge becomes an intrinsic direct band gap semiconductor, if we apply a tensile strain of about 2% [86–88, 98, 99], which is not impossible using various strain-engineering technologies in Si industries [4]. Hetero-epitaxial growth was the classical way to apply stress to the optically active layer during the growth due to the mismatch of the lattice constant [60, 61], while a tensile strain of about 0.25% is applied to Ge grown on Si by the difference in the thermal expansion coefficients between Ge and Si [5, 30, 47]. Even stronger stress can be applied by depositing a $Si_3N_4$ stress liner [100–102], or employing a membrane structure to fabricate Micro-Electro-Mechanical-Systems (MEMS) [59, 78, 103, 104]. We will discuss these stress-engineering technologies in Sec. 4.

The choice of a suitable substrate is another important aspect. Considering the cost requirement for future products, the use of a bulk Si substrate is the most attractive option. However, if we use a bulk Si substrate, the Ge light source cannot be compatible with standard Si photonic devices, which require a Silicon-On-Insulator (SOI) substrate. It will be relatively straightforward to transfer the technologies developed using Si bulk substrates to the technologies based on SOI substrates. Another substrate is a Ge-On-Insulator (GOI) substrate [105–112], which would have better crystalline quality compared with Ge directly grown on Si or SOI. The third option is the use of III-V substrate such as gallium-arsenide (GaAs) for the growth of Ge [113–116]. The lattice constants of Ge and GaAs are almost the same, and hetero-epitaxy is one of the most reliable and traditional way to make a QW. It will also be useful to investigate the impact of tensile strain [117]. These research activities would be mainly to investigate

fundamental material properties of Ge rather than near-term applications, but Ge grown on III-V materials may be useful for high-value products such as extremely efficient solar cells [116] for space applications in satellites or advanced CMOS circuits with Ge channels.

After the completion of the active layers, optical cavities [60, 61] suitable for Ge-based LDs must be designed and fabricated. FP cavities using bulk Ge WGs are simple yet useful structures [65]. For single mode operation in the future, Distributed-FeedBack (DFB) cavities or Distributed-Bragg-Reflector (DBR) mirrors will be integrated [60, 61]. For direct coupling to optical fibres, structures similar to a Vertical-External-Cavity Surface-Emitting-Laser (VECSEL) [60, 118] will be quite attractive, although the deposition of thick DBR mirrors on both sides of the substrate will be challenging, since Si CMOS processes are based on planar technologies. We can also utilize more exotic cavities like disks, rings, or Photonic-Crystals (PhCs) [60]. These cavities typically have a large quality ($Q$)-factor, compared with other cavities, therefore they are suitable for analyzing fundamental material properties as well as for applications to quantum technologies. These cavities will be reviewed in Sec. 6.

The final issue is the scheme for carrier injection. Traditional III-V LDs are based on vertical injection, since the key process technology is epitaxial growth [60]. On the other hand, for planar Si technologies, lateral carrier injection is easier to implement in terms of designs and fabrications [29, 30, 83, 101, 102]. There are many other possibilities, e.g., the combination of lateral and vertical injections [104, 118, 119].

As an example, we show in Fig. 1 (b) what kind of options we chose to make a Ge fin-type light-emitting diode (LED) [83]. We chose Ge as an active material and the structure was multi-fins, which are Multiple-Quantum-Wells (MQWs) made vertically to the substrate. In order to make the Ge fins, first, we used conventional lithography and dry etching to make Si fins. Then, RP-CVD was used to selectively grow SiGe epitaxially on top of the sidewalls of the Si fins, followed by the oxidation condensation technique [83] to make pure Ge fins [83, 120–124]. The fabricated Ge fins are expected to have better crystalline quality, since the $3D$ Ge fins can release the strain during the condensation oxidation by stretching the fins vertically to the substrate. Thus, low dark current was confirmed by lateral carrier injection [83]. In the next sections, we will review more technological details.

## 3. Active materials and structures

Active materials and their structures are one of the most important issues for Ge-based light sources, and we summarized the structure and fabrication processes in Table 1. The emission wavelengths actually depend on the stress engineering techniques, and therefore, the listed values just stand for approximate wavelengths range published in references.

**Table 1.** Active Ge structures and fabrication processes.

| Structure | $D$ | Process | Wavelengths (nm) | Reference |
|---|---|---|---|---|
| Ge on Si | 3 | 2-steps growth by UHV-CVD | $1400 \sim 2200$ | [24, 46–48, 50, 62–65] |
| Ge on Si | 3 | 2-steps growth by MBE | $1400 \sim 1700$ | [51, 66–69] |
| Ge on Si | 3 | 2-steps growth by RP-CVD | $1400 \sim 1700$ | [70–74] |
| Ge on Si | 3 | LEPE-CVD | $1400 \sim 2200$ | [75–78] |
| Ge on Si | 3 | Cold-wall thermal CVD | $1400 \sim 1700$ | [102, 125] |
| Ge on Si | 3 | MHAH by RP-CVD | - | [126] |
| Ge on Si | 3 | Hot-wire CVD | - | [127] |
| Ge on Si | 3 | Bulk Ge bonding and polishing | - | [128] |
| Ge on Si | 3 | Oxidation condensation and growth | $1400 \sim 1700$ | [129, 130] |
| Ge WG on a Si rib | 3 | RP-CVD | - | [131] |
| Ge (100) bulk | 3 | Bulk Ge substrate | $1400 \sim 2000$ | [132] |
| Ge (110) bulk | 3 | Bulk Ge substrate | - | [49] |
| n-Ge bulk | 3 | Growth by MOCVD for doping | $1400 \sim 2200$ | [133] |
| GeOI | 3 | Layer transfer with $SiO_2$ | $1500 \sim 2200$ | [105–108] |
| GeOI | 3 | Layer transfer with $Al_2O_3/SiO_2$ | $1500 \sim 2200$ | [109, 110] |
| GeOI | 3 | LPE on $Si_3N_4$ | - | [44, 134] |
| GeOI | 3 | LPE on $SiO_2$ | - | [111, 112] |
| poly-Ge on metal | 3 | MIC | - | [135] |
| Ge on GaAs | 3 | Ge on GaAs by UHV-CVD | - | [113] |
| Ge on GaAs | 3 | Ge on GaAs by MOCVD | $1400 \sim 1800$ | [114, 115] |
| SiGe/Si MQW | 2 | MBE | $1400 \sim 1700$ | [136] |
| Ge/SiGe MQW | 2 | LEPE-CVD | $1000 \sim 1300$ (10 K) | [137] |
| Ge/SiGe MQW | 2 | LEPE-CVD | $1400 \sim 1700$ | [138] |
| Ge/SiGe MQW | 2 | UHV-CVD | $1400 \sim 1700$ | [139–141] |
| Ge/SiGe MQW | 2 | RP-CVD | $1400 \sim 1600$ | [142] |
| Ge QW on IIII-V | 2 | Growth on $In_xGa_{1-x}As/GaAs$ by MBE | $1400 \sim 2000$ | [116, 117] |
| Ultrathin GOI | 2 | Oxidation condensation of $Si_{1-x}Ge_x$ | $1400 \sim 1700$ | [120–122, 124, 130, 143] |
| Ge fin | 2 | Dry etching and oxidation condensation | $1400 \sim 1700$ | [83, 84] |
| Ge fin | 2 | LPE and dry-etching | - | [44] |
| SiGe/Ge MQW | 2 | MBE | $1100 \sim 1300$ | [144] |
| a-Ge pillar | 1 | a-Ge deposition and lift-off | $1400 \sim 2600$ | [145] |
| Ge nano-wire on Si | 1 | MHAH by RP-CVD | $1400 \sim 2200$ | [110, 126] |
| Si/Ge core/shell QD | 0 | MBE | $1300 \sim 2000$ | [146] |
| Ge QD powder | 0 | Mechanical motor-grinding | $1000 \sim 1700$ | [147] |
| Ge QD on Si | 0 | Ge QDs by MBE | $1300 \sim 1600$ | [148–153] |
| SiGeSn/GeSn | 3 | UHV-CVD | - | [154] |
| GeSn/GeSi | 3 | MBE | - | [155] |
| Ge/GeSn/Ge | 3 | Double heterostructure by MBE | $1800 \sim 2300$ | [156] |
| GeSn/Ge | 3 | RP-CVD | $2000 \sim 2400$ | [55] |
| Ge/GeSn | 3 | UHV-CVD | - | [157] |

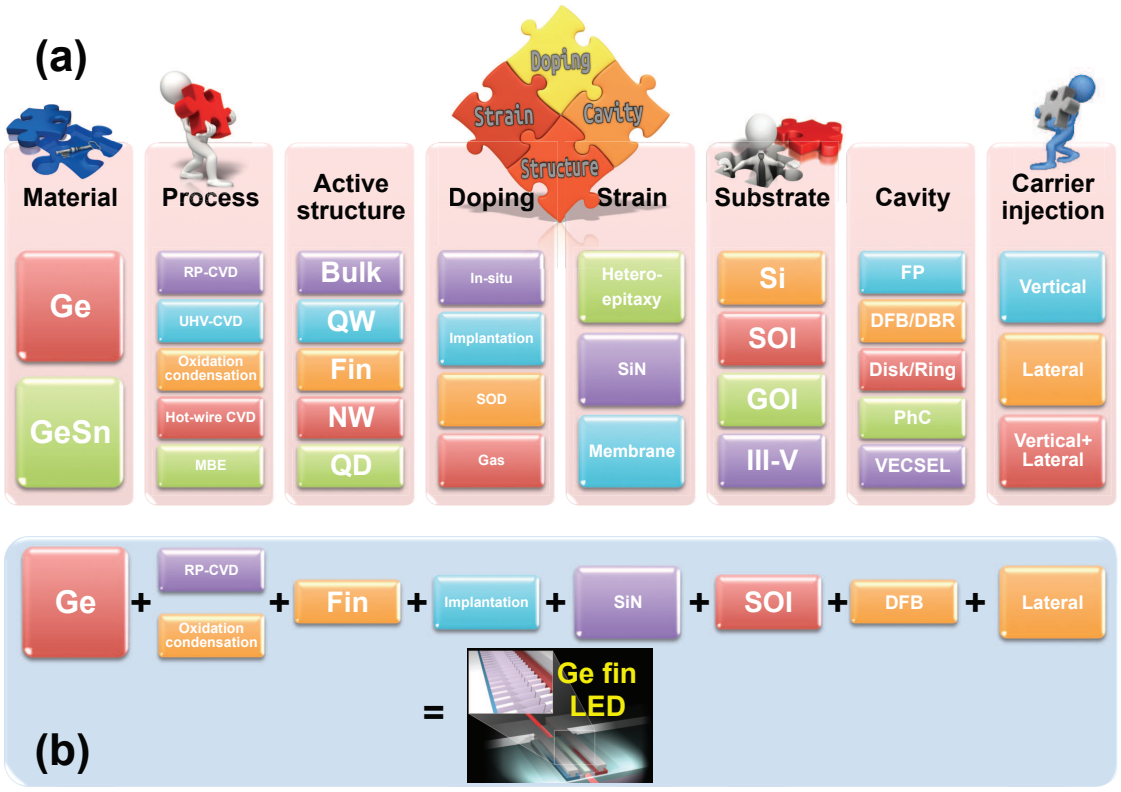


**Figure 1.** Various combinations to fabricate Ge based light sources. (a) Various options are shown for materials, fabrication processes, active structures, doping recipes, strain engineering methods, cavities structures, and carrier injection procedures. (b) An example of selected options is shown for Ge fin LED.

### *3.1. Virtual substrate: a brief history of strained Si*

The difference in the lattice constant between bulk Si and Ge is about 4.2%, which is too huge to overcome during Ge growth on Si [158–160]. The growth of single crystalline $Si_{1-x}Ge_x$ layers [158–160] is an important research area and it is still quite a challenging classical topic [27]. Here, we briefly discuss the historical background of $Si_{1-x}Ge_x$ growth technologies developed for bipolar transistors and CMOSFETs.

Under lattice-matched conditions, the epitaxially grown layer can be perfectly aligned with the original substrate, which is known as *pseudomorphic* growth [27, 158–160]. However, such growth is difficult: If the grown epi-layer exceeds the *critical thickness*, we expect significant densities of defects, such as threading dislocations, misfit dislocations, and stacking faults [27, 158–160]. The critical thickness depends on the Ge content, $x$, and larger $x$ results in smaller critical thickness, as expected [27, 158–160]. Therefore, a graded buffer layer with a gradual increase of $x$ upon growing is often prepared before the target channel layer is formed [27, 158–160]. The graded buffer layer is fully relaxed, and typically around 1-$\mu$m or more is required to secure excellent

crystalline quality [27, 158–160]. A substrate with such a graded buffer layer is called *Virtual Substrate* (VS), since we can assume the substrate is made of the crystal at the top surface (Fig. 2 (a)). Nevertheless, it has proved quite difficult to grow excellent strained-Si layer with tens of nano-meters on top of VS for application as the channels in MOSFETs due to stringent requirements to secure CMOS circuitry with billions of FETs. The wafer-scale uniform epitaxial growth process is denoted *global strain* technology, and according to the ITRS roadmap around 2000, it was expected to be introduced in mass production around 2005 [4]. However, global strain technologies have not been commonly introduced in CMOS. Instead, *local strain* technologies using $Si_3N_4$ stress liners were widely introduced around 2001, even earlier than predicted by the roadmap [161, 162].

### *3.2. Direct Ge growth on Si*

Considering the above history of global strain engineering in CMOS, it is quite surprising that Si photonic industries [18] could use a Ge PD for mass production, which is grown directly on Si [5, 27, 30, 46, 47]. There are several deposition techniques, as shown in Table 1, but the overall strategies are the same (Fig. 2 (b)). First, a thin buffer layer of Ge was deposited at Low-Tempearture (LT, $\sim$ 400 °C) directly on Si. The LT layer contains a lot of defects [46, 47]. Subsequently, the second Ge layer is deposited at High-Temperature (HT, $\sim$ 700 °C) with a higher growth rate. After deposition, post-deposition annealing is carried out [5, 30, 46, 47]. The annealing conditions are critical to improve the quality of the film, which is evidenced by increased PL intensities [102, 125]. It was reported that multiple hydrogen annealing heteroepitaxy (MHAH) [110, 126] improved the crystalline quality. Among various process technologies, RP-CVD is the commonest process in industries ready for mass production [70–74], while UHV-CVD [24, 46–48, 50, 62–65] and MBE [51, 66–69] are quite useful in universities. There are many other tools, e.g., hot-wire CVD, which is useful for the growth of a large area at low temperatures [127]. Oxidation condensation and subsequent growth is also a very interesting and unique growth technique for Si [129, 130].

### *3.3. Bulk Ge substrate and bonding to Si*

We think that gaining a fundamental understanding of material properties and physics of Ge is still important. In this regards, the use of bulk Ge substrates are useful, since we can assume almost perfect crystalline quality, while we need to think about the process technologies for transfer of the Ge light sources made on bulk Ge substrates for the future.

One concern of using bulk Ge substrates is producing an optical confinement in a cavity. The refractive index of Ge is around 4.2, and so the deposition of amorphous (a)-Si or poly-crystalline (poly)-Si does not make a WG on top of Ge. Alternatively, it was reported that a Ge bulk substrate was successfully bonded onto a Si substrate for a Ge PD at a process temperature less than 450 °C, and the Ge layer was polished to thin

down to 5.4$\mu$m [128]. This substrate would also be useful for investigating Ge-based light sources.

### *3.4. GOI*

A possible alternative technology to use a bulk Ge substrate is to make GOI by using Smart-Cut$^{TM}$ technology [163]. This involves using hydrogen (H) ion implantaion to transfer the Ge layer to the handle Si wafer with or without an oxide ($SiO_2$). In principle, this works, however, the size of available Ge wafers is much smaller than that of Si wafers, and therefore, the size limitation will prevent wafer scale bonding in larger scale production. To avoid this issue, we must transfer the grown Ge layer onto a Si substrate which has the same size of the handle wafer. Successful transfers of Ge layer grown on thick VS to make a GOI substrates was reported by several groups [105–110]. There was a concern about the weak adhesion between Ge and $SiO_2$, and existing commercially available prototypes of GOI substrates were found to be too fragile to make reliable devices [92, 107]. By using $Al_2O_3$ on top of $SiO_2$, the adhesion has been improved substantially [109, 110]. The tensile strain of Ge accumulated during the growth is usually preserved during the bonding process [107].

Liquid-Phase-Epitaxy (LPE) is also a possible option to make a local GOI structure on a Si substrate by melting Ge on top of an insulator like $Si_3N_4$ or $SiO_2$, and then re-growing single crystalline Ge through a window to the seed Si substrate [30, 44, 111, 112, 134]. Excellent single crystalline structures have been confirmed, paving the way for an investigations into the use of LPE grown Ge for light emissions.

### *3.5. Quantum wells and quantum dots*

Considering several reports on successful laser operations with bulk ($3D$) Ge [48–51] and GeSn [55], the next challenge would be to improve the performance by reducing the threshold pump power for laser operation. MQWs or QDs are suitable for reducing the threshold, and various process technologies have been used [116, 117, 136–142, 148–153]. The emission wavelength becomes slightly longer due to the quantum confinement, and therefore, applications to the wavelengths in the 1.3 $\mu$m region should be possible by optimizing the size of the quantum nano-structures. The use of fins or nano-wires by combining lithography and etching techniques could also be useful for quantum confinement [83, 84, 110, 126, 145].

### *3.6. GeSn growth*

There are two approaches for using GeSn: one is to use GeSn as an active layer with a direct band-gap [56, 57], and another is to use GeSn as a buffer layer to apply tensile-strain to Ge, which is on top of GeSn [81]. The first approach has been employed using $Si_{1-x-y}Ge_xSn_y/Ge_{1-x}Sn_x$ [154], $Ge_{1-y}Sn_y/Ge_{1-x}Si_x$ [155], $Ge/Ge_{1-x}Sn_x/Ge$ [156], and $Ge_{1-x}Sn_x/Ge$ [55]. The latter approach was taken using $Ge/Ge_{1-x}Sn_x$ [157]. For

**Table 2.** Strain-engineering technologies for Ge.

| Process | Anisotropy | Strain (%) | Reference |
|---|---|---|---|
| Thermal expansion of Ge on Si in UHV-CVD | Biaxial | 0.25 | [47, 50, 164–166] |
| Un-patterned $Si_3N_4$ on a Ge FP cavity | Uniaxial | 1.07 | [114] |
| Un-patterned $Si_3N_4$ on a Ge microdisk | Biaxial | 1 | [115] |
| Un-patterned $Si_3N_4$ on a Ge microdisk | Biaxial | 1.5 | [176] |
| Patterned $Si_3N_4$ on a Ge FP cavity | Uniaxial | 0.4 | [168] |
| Patterned $Si_3N_4$ on a Ge FP cavity | Biaxial | 0.9 | [169, 170] |
| Patterned $Si_3N_4$ on a Ge FP cavity | Biaxial | 0.4 | [102] |
| Hetero-epitaxy of Ge on $In_xGa_{1-x}As$/GaAs | Biaxial | 2.33 | [117] |
| Membrane of polyimide | Biaxial | 2.0 | [145, 167] |
| Mechanical stress on a Ge membrane | Biaxial | 0.6 | [171] |
| Ge membrane | Biaxial | 1.13 | [104] |
| Ge membrane with $Si_3N_4$ | Biaxial | 1.13 | [118] |
| Ge membrane with $Si_3N_4$ | Uniaxial | 0.98 | [106] |
| Ge bridge | Uniaxial | 2.77 | [172] |
| Ge bridge | Uniaxial | 3.1 | [78] |
| Ge bridge | Uniaxial | 5.7 | [173] |
| Ge bridge | Uniaxial | 2.3 | [110] |
| Ge microdisk on a $SiO_2$ bridge | Uniaxial | 0.92 | [177] |

both approaches, it will be required to use a double-heterostructure or similar carrier confinement structure in MQWs or QDs for practical applications, considering almost all commercially available III-V LDs are based on MQWs or QDs and do not use a bulk semiconductor as an optically active gain medium.

## 4. Strain engineering

In the last few years, significant progress has been made in understanding and technologies for strain-engineering in Ge [47, 50, 78, 92, 104, 106, 114, 115, 117, 118, 145, 164–173]. Raman spectroscopy is usually used to analyze the amount of strain from the red-shift of the phonon energy upon the application of the tensile strain [174]. The peak position of the Raman spectrum in the Bulk Ge is located at 301 $cm^{-1}$, and the shift $\Delta\omega$ is given by

$$\Delta\omega = S\epsilon, \tag{1}$$

where $\epsilon$ is the strain and $S$ is a coefficient. $S$ was reported to be 390 $cm^{-1}$ for biaxial strain [169, 170], and for uniaxial strain, $S$ was 152 $cm^{-1}$ [78, 173, 175].

Various strain-engineering technologies are summarized in Table 2 and Fig 2 and will be discussed in more detail in this section.

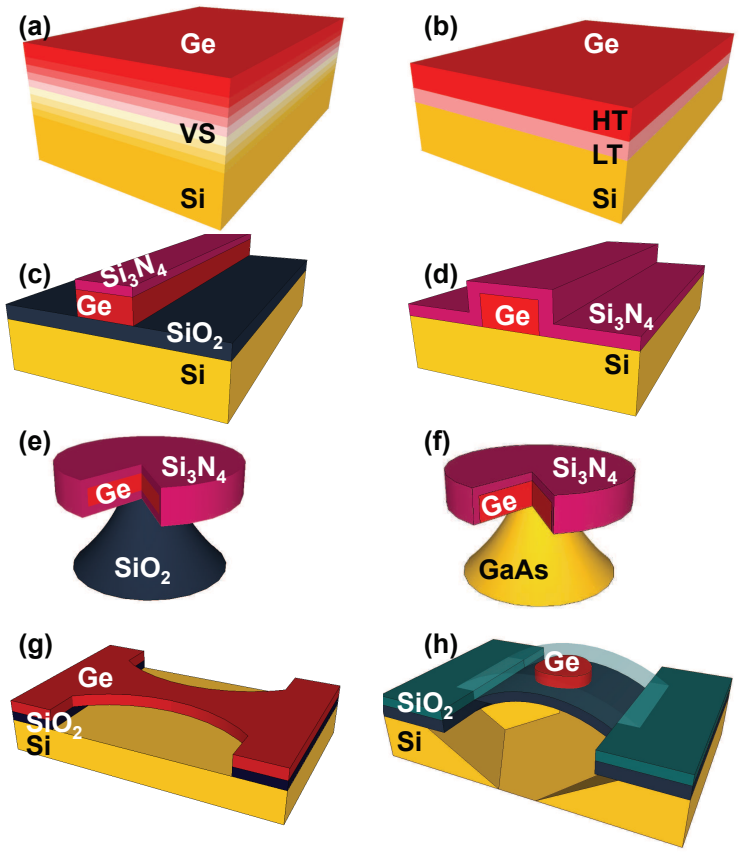


**Figure 2.** Tensile strain engineered Ge structures. (a) Epitaxially grown Ge layer on the graded buffer Virtual-Substrate (VS). (b) Two-steps grown Ge layers with the Low-Temperature (LT) grown buffer layer and the High-Temperature (HT) grown epi-layer. (c) Ge Fabry-Perot (FP) waveguide (WG) with the patterned $Si_3N_4$ stressor [169]. (d) Ge FP WG with the un-patterned $Si_3N_4$ stress liner [101]. (e) Ge microdiks with the surrounding $Si_3N_4$ stressor [176]. (f) Ge microdiks grown on GaAs with the $Si_3N_4$ stressor [115]. (g) Free-standing Ge bridge on insulator [78, 106, 172]. (h) Ge microdisk on free-standing oxide bridge [177].

### *4.1. Thermal expansion mismatch*

It is quite commonly observed that the Ge directly grown on Si has a tensile strain of around 0.25 %, using various epitaxial growth techniques including UHV-CVD [47, 50, 102, 125, 164–166], MBE [51, 66–69] RP-CVD [70–74], LEPE-CVD [75–78], Cold-wall thermal CVD [102, 125], and so on. Therefore, this is a genuine phenomenon, although it is surprising that it is a tensile strain rather than a compressive strain, since the lattice constant of bulk Ge is larger than the lattice constant of Si. This means the direct growth of Ge on Si cannot be a pseudomorphic growth with complete lattice matching between Ge and Si. The strain was expected to be relaxed in the LT layer, abut if so, why does the tensile strain remain after the growth? The mechanism was investigated, and it was found that the difference in their thermal expansion coefficients of Si and Ge is responsible for the tensile strain [47, 164], which is crucially important

for applications to Ge PDs where the efficient absorption of photons at a wavelenth of 1550-nm is key.

During the growth of a HT layer, both Ge and Si are fully relaxed at high temperatures, where no strain is expected to be remain. Then, during the cooling down to room temperature, both Ge and Si must shrink according to their respective thermal expansion coefficients. However, the thermal expansion coefficient of Ge is larger than that of Si, which means that the Ge layer must shrink more than the Si substrate, while the elastic bonds between Ge and Si will prevent deformation of the layer arriving at the fully relaxed state. As a result the lattice constant of the Ge layer must be slightly larger than that of the equilibrium point in the bulk. The expected tensile strain values depend on the starting temperature for cooling during the growth, and they were calculated in excellent agreement with experiments [164]. In fact, the remaining strain values can be controlled from compressive to tensile by increasing the post-deposition annealing temperature [5, 30, 102, 125]

### *4.2. Tensile stress liner*

It is quite natural to think about the application of *local strain* engineering technologies, using a $Si_3N_4$ stress liner [4, 161, 162] developed for CMOS to Ge-based light sources [102, 114, 115, 168–170] (Fig. 2 (c)-(f)). The internal stress of the $Si_3N_4$ stress liner can be controlled to be either compressive or tensile, depending on the hydrogen content of the film [161, 162]. Here, it is very important that the structures are patterned, otherwise the expected strain on the flat interface, which can be estimated by the famous Stoney's formula [178, 179], is very weak due to the huge difference in thickness between the stressor film and the supporting substrate. The patterning can be made into the $Si_3N_4$ layer [102, 168–170] (Fig. 2. (c)), or *vice versa* i.e., the Ge layer can be patterned, while the $Si_3N_4$ layer is un-patterned [30, 114, 115, 176] (Fig. 2. (d)-(f)).

It is also very important to recognize that the intensities of the stress strongly depend on the position. Finite-element simulations were employed to calculate the strain profile [30, 169, 177], and it was found that the stress is stronger at the interface [169] and at the corner of the WG [30]. Depending on the structures of Ge and the stressor, both tensile strained and compressive strained regions can appear within the same Ge WG [30]. This local profile of the strain would result in a local change of the band structure at the nano-scale. If the strain profile is optimally designed, the locally tensile stressed region will have a lower direct band-gap compared with the surrounding region with a type-I band alignment [172], which is similar to double-heterostructures in a III-V QW LD. This means that we cannot expect that the entire bulk Ge WG can become a direct band-gap structure, and the cladding region with a lower tensile strain or compressive strain would have a positive absorption coefficient. Therefore, the net optical gain would be significantly reduced, if the optical propagation mode in a WG has a large overlap with the lossy region. Thus, special care must be taken to design a Ge FP WG if the WG is $n$-type doped due to the increase of the free-carrier absorption. Optimistically, the

donated electrons can automatically accumulate into the region where the tensile strain is strong. Then, the actual electron concentration at the tensile stressed region can be even larger than the average impurity doping concentration, while the free electrons in the cladding region can be reduced, contributing to reduction of the loss. However, we still need to further optimize the design of the Ge FP WG, both for impurity and stress profiles.

### *4.3. Micro-bridge*

The use of a MEMS structure for applying stronger stress is attracting great attentions these days [59, 78, 104, 106, 110, 118, 145, 167, 171–173, 177]. The mechanical deformations of a free-standing bridge would certainly change the bond lengths of neighbouring Ge atoms. The theoretical proposal to use a MEMS structure for Ge light-emission was made by Lim [103]. Using finite element simulations, he showed the application of biaxial strain of the order 2 % is feasible with the possibility of positive optical gain [103]. Examples of the finite-element simulations [177] are shown in Fig. 3. Later, strong tensile-strain was actually confirmed in various free-standing membrane structures [59, 78, 104, 106, 110, 118, 145, 167, 171–173, 177].

In particular, Jain [106], Nam [172], and Süess [78] successfully fabricated micro-bridge structures almost at the same time. Their designs are quite ingenious, in which a narrow micro-bridge is connected to a wider bridge girder. As discussed in Sec. 4. 1., epitaxially grown Ge is tensile strained with about 0.25 % larger lattice expansion [164], which means that the Ge has a tendency to be compressed by its own internal force. If the wider bridge grider is movable, the force to pull the connected narrower micro-bridge is stronger, and thus a tensile strain is applied to the micro-bridge to further expand the bond length of the Ge [59, 78, 106, 110, 172, 173]. A very strong tensile-strain was confirmed, as summarized in Table 2.

While these micro-bridge ideas are interesting, it is not obvious how to combine the free standing structure with optical confinement in a cavity. One of the simplest solutions is to prepare two separate materials for a cavity and a bridge [177]. We have used the thermally grown buried-oxide (BOX) of a SOI substrate for making a micro-bridge to apply tensile-strain to the Ge micro-disk on it [177]. Whispering-Gallery-Modes (WGMs) were successfully observed from the tensely-strained Ge microdisk [177].

Another problem of the micro-bridge structure is heating while measurements due to the free-standing structure [110, 177]. Recently, Petykiewicz made a structure where the Ge bridge was bent and connected to the BOX to allow the dissipation of heat during the measurements. They successfully observed FP modes with a $Q$-factor exceeding 2,000 [110]. Exciting progress is expected along with these ideas for the future.

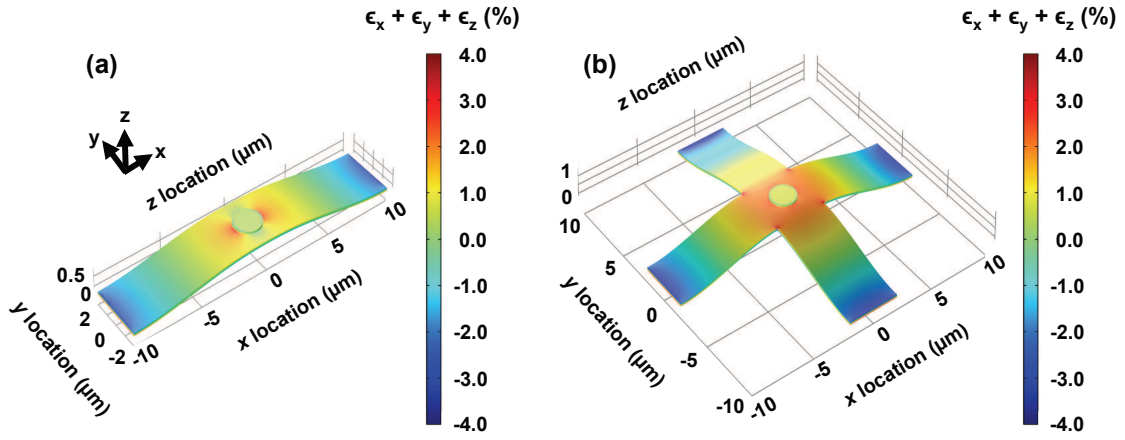


**Figure 3.** Finite-element simulations of the stress profile for (a) uniaxial beam, and (b) biaxial beam.

## 5. Electron doping

As we discussed above, $n$-type doping to fill the $L$-valley certainly enhances the spontaneous light-emission probability [86], which was confirmed by many groups and thus is well established [48, 65–69, 71, 77, 91, 92, 133, 166, 168, 180–182]. On the other hand, the impact of doping on the emergence of the optical gain is still controversial [31, 77, 110]. In fact, the crystalline qualities of actual Ge samples depend on the process technologies used, and thus the carrier life-time can vary substantially, which would affect the complex carrier dynamics upon pumping. This makes the impact of doping highly non-trivial [31, 95]. Moreover, some impurities are not activated upon doping, which would further reduce the carrier life-time, and the inhomogeneous strain profile would further affect the actual carrier profile. At this moment, there is no consensus on how much we should dope Ge with $n$-type impurities to increase the gain value.

Nevertheless, $n$-type doping has been shown to improve the quantum efficiency of LEDs. Here, we will discuss various technological options for $n$-type doping of Ge, as summarized in Table 3. In addition to the carrier concentration reported, the sheet resistance was also listed in Table 3, although the actual sheet resistance also depends on the depth of the impurity profile.

### *5.1. In-situ doping during growth*

*In situ* doping during Ge growth was reported using various processes, including UHV-CVD [65], LEPE-CVD [77], RP-CVD [133, 180], MOCVD [168], MBE [66, 184], and so on (Table 1). Independent of deposition method, there is a trade-off relationship between the crystalline quality and doping concentration, and above $2 \sim 4 \times 10^{19}$, significant degradation is observed [5, 30, 102].

**Table 3.** Process technologies to dope Ge.

| Process | Impurity | Concentration ($cm^{-3}$) | Sheet resistance ($\Omega$) | Reference |
|---|---|---|---|---|
| *In situ* by UHV-CVD | P | $1 \times 10^{19}$ | - | [65] |
| *In situ* by LEPE-CVD | P | $2.5 \times 10^{19}$ | - | [77] |
| *In situ* by RP-CVD | P | $7.5 \times 10^{18}$ | - | [71] |
| *In situ* by RP-CVD | P | $1 \times 10^{19}$ | - | [180] |
| *In situ* by MOCVD | P | $1 \times 10^{19}$ | - | [133] |
| *In situ* by MOCVD | P | $3 \times 10^{19}$ | - | [168] |
| *In situ* by MBE | Sb | $5 \times 10^{18}$ | - | [66] |
| $\delta$-doping by MBE | Sb | $2 \times 10^{20}$ | - | [183] |
| $\delta$-doping by MBE | Sb | $7 \times 10^{19}$ | - | [184] |
| $\delta$-doping by MBE | P | $1 \times 10^{20}$ | 120 | [108] |
| $\delta$-doping by UHV-CVD | P | $5 \times 10^{17}$ | - | [48] |
| $\delta$-doping by UHV-CVD and annealing | P | $4.5 \times 10^{19}$ | - | [166] |
| Multiple $\delta$-doping by MBE | P | $7.4 \times 10^{19}$ | 280 | [181] |
| Implantation | P | $6 \times 10^{19}$ | - | [185] |
| Implantation and RTA | P | - | - | [91] |
| Implantation with Co capping | P | $2.7 \times 10^{20}$ | - | [186] |
| Implantation and laser annealing | P | - | 73 | [187] |
| Implantation and laser annealing | P | - | 57 | [43] |
| Implantation and laser annealing | P | $6.5 \times 10^{19}$ | 55 | [188] |
| Co-implantation and RTA | P and Sb | $1.3 \times 10^{19}$ | - | [189] |
| Gas phase doping | As | $4 \times 10^{19}$ | - | [190] |
| GILD | P | $1.5 \times 10^{20}$ | 12 | [191] |
| GILD | P | $5 \times 10^{19}$ | - | [182] |
| SOD to bulk Ge | P | $3 \times 10^{19}$ | 36 | [192] |
| SOD to GOI | P | $1 \times 10^{19}$ | 166 | [92] |
| SOD to GOI | P | $1 \times 10^{20}$ | - | [67, 68] |
| SOD to Ge on Si | P | $4 \times 10^{19}$ | - | [69] |

### *5.2. δ-doping*

In order to overcome the trade-off, $\delta$-doping was used to achieve even higher doping concentration, while minimizing the deposition thickness of the Ge layer with poor crystalline quality [48, 108, 166, 181, 183, 184]. The $\delta$-doped layer can be removed after the diffusion to the Ge layer by Chemical-Mechanical-Polishing (CMP) [29, 166, 193]. The segregation of Sb was also controlled by optimizing the temperature during the growth to achieve a high density of active dopants [184].

### *5.3. Ion implantation*

Ion implantation is the standard process doping in Si CMOS technologies. Ge is a promising material for the channel in the future generations of CMOS technologies, and therefore researchers are developing processes of ion implantation and activation for Ge [43, 91, 185–189]. For a short channel MOSFET with a channel length as small as

10-nm, an extremely shallow junction is required to avoid the short channel effects in MOSFETs, which result in a decrease of the threshold voltage due to an increase of the leakage current [194, 195]. On the other hand, for Ge light sources, we want to dope the entire Ge layer, which may require different process optimization from the conditions for Ge MOSFETs. If we increase the power and the dose for the ion implantation, the surface of the Ge layer will become amorphous. Usually, the damaged amorphous region will be recovered by annealing [194, 195], while the crystalline quality of the bottom region underneath the a-Ge would be the LT layer with poor crystalline quality, if we use Ge directly grown on Si. If we can use the bulk Ge substrate, we will be able to recover the crystalline quality, however the issue of compatibility with SOI based Si photonics arises, again. We need more ideas to utilize ion implantation technologies for Ge light sources.

### *5.4. Gas phase doping and spin-on doping*

Considering the above difficulties of using conventional ion implantation technologies, we can think about going back to the legacy technologies based on diffusion of impurities upon heating. The gas phase doping of As was reported [190], and Gas Immersion Laser Doping (GILD) technology was developed [182, 191]. In principle, the diffusion process will enable doping up to the solid solubility density of the order of $10^{20}$ cm $^{-3}$ without significant degradation of the crystalline quality [194, 195].

SOD is another process to dope Ge with impurities from a solution based oxide [67–69, 92, 192]. In spite of the relatively simple recipes, there are several issues to do with SOD processes such as stress induced degradation of Ge due to the weak adhesion between Ge and BOX [92]. The Ge desorption as GeO during the annealing also degrades the active Ge layer [92]. By optimizing the SOD processes, a huge optical gain of 5,300 $cm^{-1}$ has been reported by Xu [69].

## 6. Optical cavities

An optical cavity is a crucial component to integrate for developments of a Ge-based LD beyond the performance of an LED, in terms of the efficiency and coherence towards practical applications [60, 61]. For short-reach optical communications, we need decent optical outputs comparable to those from III-V LDs. Then, standard optical cavities like FP, DFB, DBR, or VECSEL structures will be required [60, 61]. FP, DFB, and DBR structures can be fabricated by using a bulk Ge WG. In fact, all devices with the claims of successful laser operations are based on a bulk FP WG [48–51, 55]. Laser operations with a QW or MQWs as well as the clear experimental proof of the reproducibility from different groups will be the next academic target, while the fabrication a FP WG with embedded Ge MQWs will be quite challenging. With the GeSn-based materials, the growth of MQWs is quite promising.

For fundamental understanding and possible future applications to quantum

**Table 4.** Novel photonic cavities for Ge.

| Structure | $Q$-factor | Reference |
|---|---|---|
| Micororing on Si | 620 | [103, 197] |
| Microdisk on Si | 932 | [180] |
| Microdisk on BOX | 150 | [67] |
| Microdisk on BOX | 800 | [198, 199] |
| Microdisk on $SiO_2$ bridge | 192 | [177] |
| Free-standing microdisk | 700 | [200] |
| Free-standing microdisk | 794 | [66] |
| Free-standing microdisk | 1,350 | [115] |
| Nano-wire with DBR mirrors | 2,000 | [110] |
| PhC ring resonator | 3,085 | [153] |
| 2D PhC | 220 | [201] |
| 2D PhC | 540 | [129] |
| 2D PhC | 560 | [202] |
| 2D PhC | 600 | [203] |
| 2D PhC | 5,000 | [151] |
| 2D PhC | 16,000 | [204] |
| 3D PhC | 13,600 | [152] |

technologies, novel photonic cavities [196] would be even more suitable, as summarized in Table 3. In order to demonstrate laser operations from Ge-based light sources, the gain must be larger than the loss, while these cavities will enable a very strong optical confinement. Among them, micro-rings [103, 197] and micro-disks [66, 67, 115, 177, 180, 198–200] have very simple structures, yet exhibit high $Q$-factors of WGMs. The compatibility of optical confinements with strain-engineering has been demonstrated in Ge disks on a $SiO_2$ bridge [177] and Ge nano-wires with DBR mirrors [110].

PhC is another route to high-$Q$ cavities, and the planar processes of CMOS are quite appropriate to fabricate these PhC by using conventional lithography and dry-etching [196]. Various PhC structures are examined [129, 151–153, 201–204] with Ge QDs [151–153, 201–204] or using GOI [129]. In addition to the strong optical confinements, these cavities will enhance recombination through the Purcell effects [153, 205–212].

## 7. Applications

Future applications of Ge-based light sources are summarized in Fig. 4. The Internet-Of-Things (IOT) is expected to revolutionize the way we communicate using global sensor networks, and the demands of the communication in a data centre are exponentially increasing. It is highly desirable to realize monolithic light sources integrated on a Si photonic chip for global data centres, cloud computing, and Fibre-To-The-Home (FTTH), however severe power requirements must be overcome for applications to optical interconnections [11]. Active Optical Cables (AOCs) using Si photonics are already widely used [18], and those technologies will also be implemented in consumer

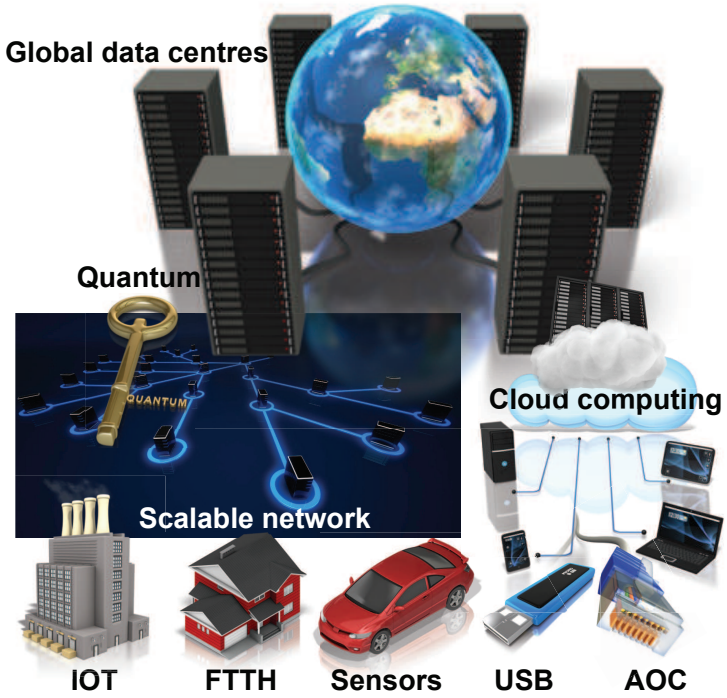


**Figure 4.** Future applications of Ge-based light sources.

products like USB memory sticks with optical input/output (I/O). The main advantage to the use of an optical interconnection rather than metal wiring is the power reduction in addition to the higher data transmission rate. A quantum efficiency as high as that of a III-V LD is required for it to be replaced by a Ge-based LD. If the developed Ge LD in the future can be operated very fast, which means at least as fast as 10-Gbps and ideally beyond 25-Gbps, direct modulation without using a modulator will be possible. In that case, the energy consumption estimated for a modulator will not be needed, which would slightly relax the requirement for the quantum efficiency.

There are many other possible applications of Ge-based light sources, like Local-Area-Network (LAN) in cars or bio-sensing. For these applications, a laser operation may not be necessary, as far as the quantum efficiency of Ge-based LED is reasonable. For example, a LED is used for LAN in a car, due to the relatively slow data rate of around 25 Mbps. The advantage of using Ge-based light sources will be the cost and the integration capabilities using CMOS processes. Applications to quantum technologies as a single photon source will also be interesting. It will be very important to identify the first target for a real product of Ge-based light sources.

## 8. Conclusion

We have reviewed the current status of the developments of Ge-based light sources towards monolithic integration in a Si chip. There are so many technological options for

fabricating Ge-based light sources. Suitable material choice and design of the structure will be very important, and epitaxial growth processes should be further improved with the help of various patterning techniques. Stress-engineering and doping will be further developed to increase the optical gain values upon pumping. The optical confinements must be considered together with the structure of the active layer and the scheme of carrier injections. At this moment, there is no standard process to fabricate Ge-based light sources, and more innovative ideas are needed. We would like to encourage more researchers ranging from condensed-matter physicists to process/device engineers to join this rapidly growing area.

## Acknowledgments

We would like to thank our collaborators, especially, Tani K, Okumura T, Ido T, Kako S, Prof Iwamoto S, and Prof Arakawa Y. We are also grateful to Prof Rutt H N and Boden S for their proof reading of manuscript and constructive comments. This work is supported by EPSRC Standard Grant (EP/M009416/1), EPSRC Manufacturing Fellowship (EP/M008975/1), EU FP7 Marie-Curie Carrier-Integration-Grant (PCIG13-GA-2013-618116), and the University of Southampton Zepler Institute Research Collaboration Stimulus Fund.

## Appendix A. List of abbreviations

| | |
|---|---|
| AOC | Active Optical Cable |
| BOX | Buried OXide |
| CMOS | Complementary Metal-Oxide-Semiconductor |
| CMP | Chemical-Mechanical-Polishing |
| D | Dimensional |
| DBR | Distributed-Bragg-Reflector |
| DFB | Distributed-FeedBack |
| EM | Electro-Magnetic |
| FET | Field-Effect Transistor |
| FP | Fabry-Perot |
| FTTH | Fibre-To-The-Home |
| GaAs | Gallium Arsenide |
| Ge | Germanium |
| GeSn | Germanium-Tin |
| GILD | Gas Immersion Laser Doping |
| H | Hydrogen |
| IC | Integrated Circuit |
| I/O | Input/Output |
| IOT | Internet-Of-Things |
| III-V | group III-V compound semiconductor |
| InGaAs | Indium Gallium Arsenide |
| LAN | Local-Area Network |
| LED | Light-Emitting Diode |
| LEPE-CVD | Low-Energy Plasma-Enhanced Chemical Vapour Deposition |
| LPCVD | Low Pressure Chemical Vapour Deposition |
| LPE | Liquid Phase Epitaxy |
| LSI | Large-scale Integrated Circuit |
| MBE | Molecular Beam Epitaxy |
| MEMS | Micro Electro Mechanical Systems |
| MHAM | Multiple Hydrogen Annealing Heteroepitaxy |
| MIC | Metal-Induced Crystallization |
| MQW | Multiple Quantum Well |
| MOCVD | Metal-Organic Chemical Vapour Deposition |
| MOS | Metal-Oxide-Semiconductor |
| NIR | Near-infrared |
| PhC | Photonic Crystal |
| QM | Quantum Mechanical |
| RP-CVD | Reduced Pressure Chemical Vapour Deposition |
| RTA | Rapid Thermal Annealing |
| SOD | Spin-On Dopant |
| SOI | Silicon On Insulator |
| Si | Silicon |
| SiGe | Silicon Germanium |
| UHV-CVD | Ultra-High Vacuum Chemical Vapour Deposition |
| VECSEL | Vertical-External-Cavity Surface-Emitting-Laser |
| WG | Waveuuide |
| WGM | Whispering-Gallery-Mode |

## Appendix B. Introduction to quantum field theory for spontaneous and stimulated emissions

The generation of an elementary particle, a photon, by recombination of an electron and its anti-particle, a hole, in a semiconductor is a highly Quantum Mechanical (QM) phenomenon. However, the modern quantum field theoretical treatments in condensed matter physics are not necessarily popular among engineers working for CMOS and Si photonics. Therefore, we briefly review the second quantized formulation for spontaneous and stimulated emissions, which are suitable to analyse the gain for bulk Ge. Interested readers should follow more advanced textbooks [61, 213].

In general, many body Hamiltonian for electrons is described by

$$H = \sum_{i,j} \langle i|\mathcal{H}|j\rangle c_i^\dagger c_j, \tag{B.1}$$

where $c_i^\dagger$ and $c_i$ are the creation and annihilation operators for the $i$-th state, which run over all states including spins $\sigma$, and $\langle i|\mathcal{H}|j\rangle$ is the one-body Hamiltonian, which becomes in the coordinate representation

$$\langle \mathbf{x}|\mathcal{H}|\mathbf{x}'\rangle = \left[-\frac{\hbar^2\nabla^2}{2m_\mathrm{e}} + V_\mathrm{lattice}(\mathbf{x})\right]\delta(\mathbf{x}-\mathbf{x}'), \tag{B.2}$$

where $m_\mathrm{e}$ is the bare electron mass in a vacuum, and $V_\mathrm{lattice}(\mathbf{x})$ is a periodic potential from a crystal lattice.

The one-body problem can be solved by the $\mathbf{k}\cdot\mathbf{p}$ method or *ab initio* calculations, and the solution of the Schrödinger Eq.

$$\left[\frac{\mathbf{p}^2}{2m_\mathrm{e}} + V_\mathrm{lattice}(\mathbf{x})\right]\psi_i(\mathbf{x}) = \epsilon_i\psi_i(\mathbf{x}), \tag{B.3}$$

is given by the Bloch state

$$\psi_{\mathbf{k}n}(\mathbf{x}) = u_{\mathbf{k}n}(\mathbf{x})\frac{\mathrm{e}^{i\mathbf{k}\cdot\mathbf{x}}}{\sqrt{V}}, \tag{B.4}$$

where $u_{\mathbf{k}n}$ describes the rapidly oscillating atomic wavefunction, for the $n$-th band with the band dispersion, $\epsilon_{\mathbf{k}n}$, and $V$ is the volume of a bulk active material. Then, the Hamiltonian for electrons without the electro-magnetic (EM) fields is given by

$$H_0 = \sum_{\mathbf{k}n\sigma}(\epsilon_{\mathbf{k}n} - E_{\mathrm{F}n})c_{\mathbf{k}n\sigma}^\dagger c_{\mathbf{k}n\sigma}, \tag{B.5}$$

where $E_{\mathrm{F}n}$ is the quasi-Fermi level (more precisely, chemical potential) for the $n$-th band. What is unusual in a semiconductor, is we can apply different Fermi levels for the conduction band ($E_\mathrm{Fc}$) and the valence band ($E_\mathrm{Fv}$) by electrical or optical pumping. Fortunately, the non-interacting many-body Hamiltonian $H_0$ can be solved exactly and the partition function, $Z$, is given by

$$Z = \prod_{\mathbf{k}n\sigma} \exp\left(-\frac{\sum_{\mathbf{k}n\sigma}(\epsilon_{\mathbf{k}n} - E_{\mathrm{F}n})n_{\mathbf{k}n\sigma}}{kT}\right), \tag{B.6}$$

considering all the possible combinations of states, which are occupied $n_{\mathbf{k}n\sigma} = 1$ or not $n_{\mathbf{k}n\sigma} = 0$. As a result, we can calculate all thermodynamic properties, including the

statistical QM occupation probabilities for the conduction band $\epsilon_{\mathbf{kc}}$ and the valence band $\epsilon_{\mathbf{kv}}$

$$\langle c^\dagger_{\mathbf{kc}\sigma} c_{\mathbf{kc}\sigma}\rangle = \frac{1}{1+\exp(-\frac{\epsilon_{\mathbf{kc}}-E_{\mathrm{Fc}}}{kT})} \equiv f_{\mathrm{c}}(\epsilon_{\mathbf{kc}}) \tag{B.7}$$

$$\langle c^\dagger_{\mathbf{kv}\sigma} c_{\mathbf{kv}\sigma}\rangle = \frac{1}{1+\exp(-\frac{\epsilon_{\mathbf{kv}}-E_{\mathrm{Fv}}}{kT})} \equiv f_{\mathrm{v}}(\epsilon_{\mathbf{kv}}), \tag{B.8}$$

which are both given by Fermi-Dirac distribution functions.

Similarly, the classical EM Hamiltonian in a bulk semiconductor of the dielectric constant of $\epsilon$,

$$H_{\mathrm{EM}} = \int_V d^3\mathbf{x}\left(\frac{\epsilon}{2}\mathbf{E}^*(\mathbf{x})\cdot\mathbf{E}(\mathbf{x}) + \frac{1}{2\mu_0}\mathbf{B}^*(\mathbf{x})\cdot\mathbf{B}(\mathbf{x})\right), \tag{B.9}$$

can be diagonalized to obtain the second quantized form

$$H_{\mathrm{EM}} = \sum_{\mathbf{k}s}\hbar\omega_k\left(b^\dagger_{\mathbf{k}s}b_{\mathbf{k}s} + \frac{1}{2}\right), \tag{B.10}$$

where $b^\dagger_{\mathbf{k}s}$ and $b_{\mathbf{k}s}$ describe the creation and the annihilation operators for a photon with the polarization $s$ (1 or 2). This can be achieved by inserting the vector potential

$$\mathbf{A}(\mathbf{x},t) = \sum_{\mathbf{q}s}\sqrt{\frac{\hbar}{2\epsilon\omega_q V}}\mathbf{e}_s\left(b_{\mathbf{k}s}\mathrm{e}^{i\mathbf{k}\cdot\mathbf{x}-i\omega t} + b^\dagger_{\mathbf{k}s}\mathrm{e}^{-i\mathbf{k}\cdot\mathbf{x}+i\omega t}\right), \tag{B.11}$$

into the electric field $\mathbf{E}(\mathbf{x},t) = -\partial\mathbf{A}(\mathbf{x},t)/\partial t$ and the magnetic field $\mathbf{B}(\mathbf{x},t) = \nabla\times\mathbf{A}(\mathbf{x},t)$ under the Coulomb gauge $\nabla\cdot\mathbf{A}(\mathbf{x},t) = 0$.

The electron-photon interaction can be generated by via the electron charge of $-e$ through $\mathbf{A}(\mathbf{x},t)$, in the Schrödinger Eq.

$$\left[\frac{(\mathbf{p}+e\mathbf{A}(\mathbf{x},t))^2}{2m_{\mathrm{e}}} + V_{\mathrm{lattice}}(\mathbf{x})\right]\psi_i(\mathbf{x}) = \epsilon_i\psi_i(\mathbf{x}), \tag{B.12}$$

and therefore, the one-body interaction Hamiltonian is

$$\mathcal{H}_{\mathrm{int}}(\mathbf{x}) = \frac{e}{m_{\mathrm{e}}}\mathbf{A}(\mathbf{x},t)\cdot\mathbf{p}, \tag{B.13}$$

which can be converted to show

$$\mathcal{H}_{\mathrm{int}}(\mathbf{x}) = e\mathbf{E}(\mathbf{x},t)\cdot\mathbf{x} \equiv -\mathbf{E}(\mathbf{x},t)\cdot\mu, \tag{B.14}$$

that the EM waves couple and oscillate the electric dipole $\mu = -e\mathbf{x}$. Therefore, light-emissions by the recombinations of electrons and holes are described by the dipole radiations.

By inserting the field operators, we obtain the interaction Hamiltonian,

$$H_{\mathrm{int}} = \sum_{\mathbf{k}\mathbf{q}s\sigma}\sqrt{\frac{\hbar}{2\epsilon\omega_{\mathbf{q}}V}}\left(\mathbf{e}_s\cdot\mathbf{p}_{\mathrm{vc}}\mathrm{e}^{i\omega t}b^\dagger_{\mathbf{q}s}c^\dagger_{\mathbf{k}+\mathbf{q}\mathrm{v}\sigma}c_{\mathbf{kc}\sigma} + \mathbf{e}_s\cdot\mathbf{p}_{\mathrm{cv}}\mathrm{e}^{-i\omega t}b_{\mathbf{q}s}c^\dagger_{\mathbf{k}+\mathbf{q}\mathrm{c}\sigma}c_{\mathbf{kv}\sigma}\right), \tag{B.15}$$

where the first (second) term describes the emission (absorption) of a photon through the collision between an electron in the conduction band and a hole in the valence band.

We have defined the optical transition matrix element by the integral over the unit cell of the volume $V_{\rm uc}$

$$\mathbf{p}_{\rm vc} = \frac{1}{V_{\rm uc}} \int_{V_{\rm uc}} d^3\mathbf{x} u_{\rm v}^*(\mathbf{x}) \mathbf{p} u_{\rm c}(\mathbf{x}), \tag{B.16}$$

which describes the optical selection rules, requiring the change of the *parity* and the conservation of the angular momentum, provided by the unit spin of a photon. Note that the momentum is conserved during the collision processes, while the momentum of a photon is low and $\mathbf{q} \sim \mathbf{0}$ dominates without changing the momentum of an electron and a hole.

After obtaining $H_{\rm int}$, the QM average of the emission and absorption rates from the initial state $i$ to the final state $f$ can be calculated by Fermi's Golden rule,

$$w_{i\to f}^{\rm QM} = \frac{2\pi}{\hbar} |\langle f|H_{\rm int}|i\rangle|^2 \delta(E_f - E_i \pm \hbar\omega), \tag{B.17}$$

where $+$ $(-)$ stands for emissions (absorptions), and the energy conservation is required upon recombinations. To calculate the matrix element, we must remember that each many-body state is described by the direct product of an electronic state and a photonic state. For electronic states, we must also take the statistical average into account for electronic states. In order to calculate the emission rate, the conduction band must be occupied and the valence band must be occupied whose statistical average will give a factor of

$$f_{\rm c}(\epsilon_{\mathbf{k}\rm c})\Big(1 - f_{\rm v}(\epsilon_{\mathbf{k}\rm v})\Big), \tag{B.18}$$

while the absorption process will give a factor of

$$f_{\rm v}(\epsilon_{\mathbf{k}\rm v})\Big(1 - f_{\rm c}(\epsilon_{\mathbf{k}\rm c})\Big), \tag{B.19}$$

On the other hand, a photonic state can be considered to be an essentially pure QM state at zero temperature except for the black body radiations. The matrix element of the bosonic creation operator will give a factor of

$$\langle n_{\mathbf{q}s} + 1|b_{\mathbf{q}s}^\dagger|n_{\mathbf{q}s}\rangle = \sqrt{n_{\mathbf{q}s} + 1}, \tag{B.20}$$

for the emission process, while for the absorption process it is

$$\langle n_{\mathbf{q}s} - 1|b_{\mathbf{q}s}|n_{\mathbf{q}s}\rangle = \sqrt{n_{\mathbf{q}s}}. \tag{B.21}$$

This difference is especially important, since this explains the difference between spontaneous and stimulated emissions. For spontaneous emissions, a photon is produced from the vacuum where there is no photon,

$$\langle 1|b_{\mathbf{q}s}^\dagger|0\rangle = 1. \tag{B.22}$$

Thus, a photon is created even without any net average electric fields, while there are vacuum zero-point fluctuations (Fig. B1 (a)). In stimulated emissions, the number of photons will be increased (or decreased) by the electric fields created by the photons themselves (Fig. B1 (b)), which are trapped in a cavity. Successive productions of copies of photons with the same phase can achieve the macroscopic occupation of the single

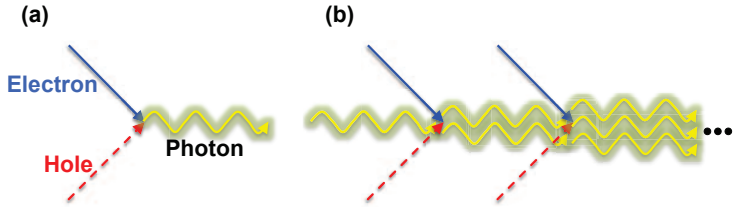


**Figure B1.** Feynman diagram for (a) spontaneous and (b) stimulated emissions.

mode, which is considered to be a Bose-Einstein condensation of photons. Therefore, the radiation from a laser is coherent.

Finally, the total emission and absorption rates are

$$W^{\text{emission}} = \frac{2\pi}{\hbar}\frac{e^2}{m_{\text{e}}}\frac{\hbar}{2\epsilon\omega_q}\frac{1}{V}\sum_{\mathbf{k}\sigma}(n_{\mathbf{q}s}+1)|\mathbf{e}_s\cdot\mathbf{p}_{\text{vc}}|^2 f_{\text{c}}(\epsilon_{\mathbf{kc}})\Big(1-f_{\text{v}}(\epsilon_{\mathbf{kv}})\Big)\delta(\epsilon_{\mathbf{kv}}-\epsilon_{\mathbf{kc}}+\hbar\omega) \tag{B.23}$$

$$W^{\text{absorption}} = \frac{2\pi}{\hbar}\frac{e^2}{m_{\text{e}}}\frac{\hbar}{2\epsilon\omega_q}\frac{1}{V}\sum_{\mathbf{k}\sigma} n_{\mathbf{q}s}|\mathbf{e}_s\cdot\mathbf{p}_{\text{cv}}|^2 f_{\text{v}}(\epsilon_{\mathbf{kv}})\Big(1-f_{\text{c}}(\epsilon_{\mathbf{kc}})\Big)\delta(\epsilon_{\mathbf{kc}}-\epsilon_{\mathbf{kv}}-\hbar\omega). \tag{B.24}$$

Therefore, we obtain spontaneous and stimulated emission rates

$$W^{\text{spon.}} = \frac{2\pi}{\hbar}\frac{e^2}{m_{\text{e}}}\frac{\hbar}{2\epsilon\omega_q}\frac{1}{V}\sum_{\mathbf{k}\sigma}|\mathbf{e}_s\cdot\mathbf{p}_{\text{vc}}|^2 f_{\text{c}}(\epsilon_{\mathbf{kc}})\Big(1-f_{\text{v}}(\epsilon_{\mathbf{kv}})\Big)\delta(\epsilon_{\mathbf{kv}}-\epsilon_{\mathbf{kc}}+\hbar\omega) \tag{B.25}$$

$$W^{\text{stim.}} = \frac{2\pi}{\hbar}\frac{e^2}{m_{\text{e}}}\frac{\hbar}{2\epsilon\omega_q}\frac{1}{V}\sum_{\mathbf{k}\sigma} n_{\mathbf{q}s}|\mathbf{e}_s\cdot\mathbf{p}_{\text{cv}}|^2\Big(f_{\text{c}}(\epsilon_{\mathbf{kc}})-f_{\text{v}}(\epsilon_{\mathbf{kv}})\Big)\delta(\epsilon_{\mathbf{kc}}-\epsilon_{\mathbf{kv}}-\hbar\omega), \tag{B.26}$$

respectively.

Considering the optical power density of $P=\hbar\omega_{\mathbf{q}}v_{\text{g}}n_{\mathbf{q}s}$, where the group velocity is $v_{\text{g}}=c/n_{\text{r}}$ with the refractive index of $n_{\text{r}}$, we can obtain the gain formula

$$g = \frac{W^{\text{stim.}}/V}{P/(\hbar\omega)} \tag{B.27}$$

$$= \frac{\pi e^2}{m_{\text{e}}^2 n_{\text{r}}\epsilon_0 c\epsilon\omega_q}\frac{1}{V}\sum_{\mathbf{k}\sigma}|\mathbf{e}_s\cdot\mathbf{p}_{\text{cv}}|^2\Big(f_{\text{c}}(\epsilon_{\mathbf{kc}})-f_{\text{v}}(\epsilon_{\mathbf{kv}})\Big)\delta(\epsilon_{\mathbf{kc}}-\epsilon_{\mathbf{kv}}-\hbar\omega). \tag{B.28}$$

We have not explicitly included the degeneracy of valence bands with heavy holes and light holes, but it is straightforward to includes these contributions. The inclusion of the $L$-valley in the conduction band will reduce the gain values significantly due to the free carrier absorptions, while helping the populations in the $\Gamma$ valley. The quantitative evaluations are currently hot topics in the area of Ge light-emissions.

## Appendix C. Optical mode confinement in a Fabry-Perot waveguide : an analogy of photonics with electronics

The starting fundamental equations to describe the electromagnetic waves in a dielectric with the refractive index of $n$ are Maxwell's equations, or their equivalent relativistic form of Poisson Eq.

$$\left(\nabla^2 - \frac{1}{v^2}\right)\mathbf{E} = 0, \tag{C.1}$$

where $v = c/n$ is the velocity of a photon in a dielectric, which is slower than that in vacuum, $c$. If a photon is propagating along $z$ with the polarization along $x$, the solution in a uniform dielectric is given by

$$E_x \sim \mathrm{e}^{i(\omega t - k_z z)}, \tag{C.2}$$

with the simple *massless* photon dispersion relationship of $\omega = vk_z$ between angular frequency $\omega$ and the wavenumber $k_z$.

In our Si photonics applications, the refractive index depends on the positions (x,y) perpendicular to a FP WG [6–10]. Then, the Poisson Eq. for the Transverse-Electric (TE) mode, $E_x^j \mathrm{e}^{i(\omega t - k_z^j z)}$, becomes

$$\left(\partial_x^2 + \partial_x^2 - k_z^{j2} + \frac{n(x,y)^2}{c^2}\omega^2\right)E_x^j(x,y) = 0, \tag{C.3}$$

for the $j$-th eigenmode. A similar equation is also valid for the Transverse-Magnetic (TM) mode. By substituting with $k_z^j = \omega n_{\mathrm{eff}}^j/c$, we obtain

$$\left(\partial_x^2 + \partial_x^2 - \frac{\omega^2}{c^2}\left(n_{\mathrm{eff}}^{j2} - n(x,y)^2\right)\right)E_x^j(x,y) = 0. \tag{C.4}$$

We can compare Eq. (C.4) with the 2D Schrödinger equation with the effective mass of $m_{\mathrm{eff}}$ under the potential $V_{\mathrm{eff}}(x,y)$, whose discrete energy level is $E_{\mathrm{eff}}^j$,

$$\left(\partial_x^2 + \partial_x^2 - \frac{2m_{\mathrm{eff}}}{\hbar^2}\left(V_{\mathrm{eff}}(x,y) - E_{\mathrm{eff}}^j\right)\right)\psi(x,y) = 0, \tag{C.5}$$

and we get intuitive Eqs

$$V_{\mathrm{eff}}(x,y) = -\hbar\omega n(x,y)^2 \tag{C.6}$$

$$E_{\mathrm{eff}}^j = -\hbar\omega n_{\mathrm{eff}}^{j2} \tag{C.7}$$

$$m_{\mathrm{eff}}c^2 = \frac{\hbar\omega}{2}. \tag{C.8}$$

This means that a photon propagating along with a FP WG becomes *massive* perpendicular to the WG, and we have the emergence of the *rest* effective mass with the Einstein relationship for the zero-point energy. Moreover, the squared refractive index with a negative sign works as an effective attractive potential for a photon, which means a photon has a tendency to be trapped in a material with a higher refractive index. For example, assuming the photon energy of $\hbar\omega = 1$ eV, we get $m_{\mathrm{eff}} = 0.976 \times 10^{-6} m_{\mathrm{e}}$, where $m_{\mathrm{e}}$ is the bare electron mass, which means the effective mass of a photon is 6-orders of magnitude smaller than that of an electron. This estimation is also consistent

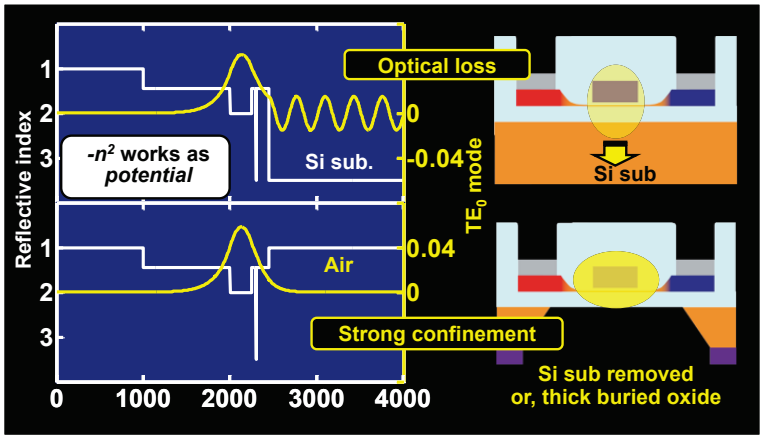


**Figure C1.** Quantum mechanical behaviours of a photon propagating in a waveguide. A $Si_3N_4$ waveguide is fabricated on top of a Ge quantum-well with a thin buried oxide. (a) Leakage of the propagating mode into the substrate through the thin buried oxide. (b) Stronger confinement in a waveguide due to the local removal of the substrate.

with the difference of the rest energies between a photon $m_{\rm eff}c^2 = \hbar\omega/2 = 0.5$-eV and an electron $m_{\rm e}c^2 = 0.512$-MeV.

As an application of this formulation, we can think about the tunnelling leakage from the waveguide to the substrate (Fig. C1). The tunnelling leakage probabilities from the false vacuum can be calculated by the *instanton* method [214], which is equivalent to the Wentzel-Kramers-Brillouin (WKB) formula,

$$\Gamma \sim {\rm e}^{-\frac{B}{\hbar}}, \tag{C.9}$$

where

$$B = \oint \sqrt{2m_{\rm eff}(V_{\rm eff}(x,y) - E^j_{\rm eff})}\, dy. \tag{C.10}$$

According to the above estimation of the effective mass, in order to avoid the optical leakage, we need to prepare the cladding layer with a thickness of approximately 3-orders of magnitude larger than that of an electronic system. In fact, the tunnelling of electrons can be observed in a commercially available MOS with a gate oxide thickness of around 1-nm, while the cladding layer of the Si WG and the box thickness should be around 1-$\mu$m.

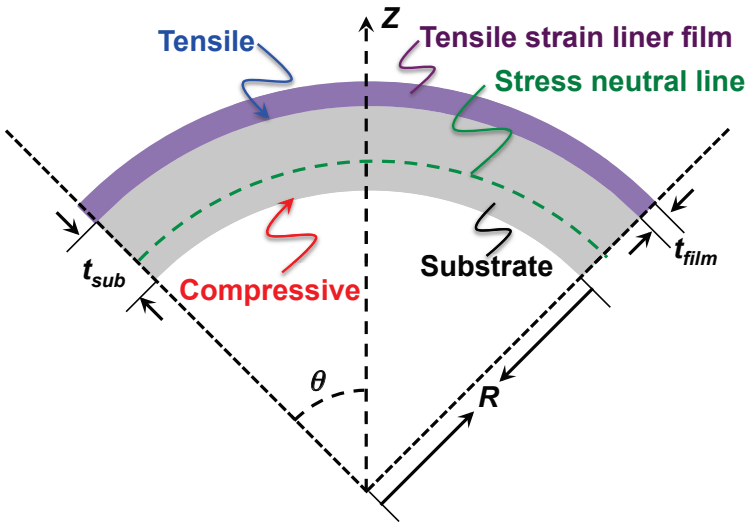


**Figure D1.** Deformation of a wafer after the deposition of the tensile stress liner.

## Appendix D. Derivation of Stoney's formula

Stoney's formula [178, 179], which was derived in 1909, is quite useful to estimate the *global* strain of the stress liner film. For the *local* strain, we need finite-element simulations. Nevertheless, Stoney's formula is still valuable to estimate the internal stress of the deposited film, experimentally, and it will be also useful in understanding how the deformation will be induced by the film with an internal stress. Therefore, we will derive Stoney's formula in this appendix.

Suppose we have a bulk substrate, which is a Ge or Si substrate in our case, with a thickness of $t_{\rm sub}$. We will deposit a film with the thickness of $t_{\rm film}$ with an internal stress of $\sigma_{\rm film}$, as shown in Fig. D1. Here, we assume that the surface of the substrate is *tensely-strained*, which means the atomic bond length is expanded, compared with the lattice constant in the bulk. For this inward bending, the deposited film has a tendency to expand, which means that the film is *compressively-strained*, internally. The force is always balanced by the action-reaction law, i.e. Newton's third law of motion, so that the words of tensile and compressive are sometimes confusing. Fortunately, both compressive and tensile stress liners are available in CMOS processes prepared for both $n$-MOS and $p$-MOS. Of course, the bending will be outward, if we deposit the film with an internal *tensile strain*.

If we use $X_i$ and $X_i'$ for positions before and after the displacement in the elastic body, the local displacement is described by $u_i = X_i' - X_i$, where $i = x, y, z$. The deformation is described by the strain tensor

$$u_{ik} = \frac{1}{2}\left(\frac{\partial u_i}{\partial x_k} + \frac{\partial u_k}{\partial x_i}\right), \tag{D.1}$$

where $i, k = x, y, z$.

For example, by using the Yang's modulus, $E$, and the Poisson ratio, $\nu$, the deformation by the uniaxial compressive stress $P$ along $z$ can be described as

$$u_{zz} = -\frac{1}{E}P \tag{D.2}$$

$$u_{xx} = u_{yy} = -\nu u_{zz} = \frac{\nu}{E}P. \tag{D.3}$$

Similarly, the biaxial strain, $\sigma_{xx} = \sigma_{yy} = \sigma$ along the $xy$ plane, will induce the deformation of

$$u_{xx} = u_{yy} = \frac{1-\nu}{E}\sigma \tag{D.4}$$

$$u_{zz} = -\frac{2\nu}{E}\sigma. \tag{D.5}$$

In other words, we can define biaxial modulus, $E_{\mathrm{b}}$, for the biaxial strain as

$$E_{\mathrm{b}} = \frac{E}{1-\nu}, \tag{D.6}$$

which means that the displacement will be larger than the uniaxial strain, because the elastic body is bent along 2 directions.

Going back to the original problem of the inward bending in Fig. D1 with the bending radius of $R$, the top surface of the substrate is tensely-strained, while the bottom of the substrate is compressively strained. This is apparent, because the length of the arc at the top surface, $2(R + t_{\mathrm{film}})\theta$, is larger than the original diameter of the substrate, while the bottom length of the arc, $2R\theta$, is shorter than that. Now, the strain profile is not uniform across the wafer, and it depends on the location along $z$, where we take the origin of $z$ at the bottom of the substrate. There exists the stress neutral line at $z = z_0$, where the internal stress is negligible. Assuming the uniform deformation from the neutral line, the strain tensor can be calculated from the ratio of the length of the arc as

$$u_{xx} = u_{yy} \tag{D.7}$$

$$= \frac{2(R+z)\theta - 2(R+z_0)\theta}{2(R+z_0)\theta} \tag{D.8}$$

$$\approx \frac{z - z_0}{R} \tag{D.9}$$

Then, the biaxial strain in the substrate depends on the depth, $z$, and we obtain it as

$$\sigma_{\mathrm{sub}} = \frac{E}{1-\nu}\frac{z - z_0}{R}. \tag{D.10}$$

At the top surface of the substrate, $z = t_{\mathrm{sub}}$, the bending moment is zero, since the elastic body is not rotating, which leads

$$\int_0^{t_{\mathrm{sub}}} (z - t_{\mathrm{sub}})\sigma_{\mathrm{sub}}\, dz = 0. \tag{D.11}$$

Then, we obtain the stress neutral position

$$z_0 = \frac{1}{3}t_{\mathrm{sub}}. \tag{D.12}$$

We also have the following identity, which is coming from the balance of the force between the substrate and the film, as

$$\int_0^{t_{\rm sub}} \sigma_{\rm sub}\, dz = \int_{t_{\rm sub}}^{t_{\rm sub}+t_{\rm film}} \sigma_{\rm film}\, dz. \tag{D.13}$$

After integrating both sides, we finally obtain the Stoney's formula

$$\sigma_{\rm film} = \frac{E}{1-\nu}\frac{t_{\rm sub}^2}{6t_{\rm film}R}, \tag{D.14}$$

which is useful in estimating the strain from $R$.

It is evident from Eq. (D.10), that the tensile strain is maximized at the top surface

$$\sigma_{\rm sub}(t_{\rm sub}) = \frac{E}{1-\nu}\frac{2t_{\rm sub}}{3R}, \tag{D.15}$$

while it is compressive at the bottom as

$$\sigma_{\rm sub}(0) = -\frac{E}{1-\nu}\frac{t_{\rm sub}}{3R}. \tag{D.16}$$

If we calculate the ratios of Eqs. (D.15) and (D.16) to (D.14), we obtain

$$\frac{\sigma_{\rm sub}(t_{\rm sub})}{\sigma_{\rm film}} = \frac{4t_{\rm film}}{t_{\rm sub}}, \tag{D.17}$$

$$\frac{\sigma_{\rm sub}(0)}{\sigma_{\rm film}} = -\frac{2t_{\rm film}}{t_{\rm sub}}, \tag{D.18}$$

which means that the impact of a uniform film on a bulk substrate is extremely weak, as long as we are using a standard substrate with a thickness of 100 $\sim$ 800-$\mu$m, with a stressor film of thickness less than 1-$\mu$m. We can apply a greater strain if we thin down the wafer with mechanical bending [171]. We can also recognize that the use of a MEMS architecture like a bridge is quite valuable, since the thickness of the bridge is comparable to the thickness of the strained-layer, thus, we can expect significant application of the strain to the active Ge [78, 106, 172, 177].

[1] Feynman R P 1992 (The transcript of a talk in 1959 at the annual meeting of the American Physical Society (APS)) *IEEE J. Microelectromechanical Systems* **1** 60–66
[2] Kilby J S C 1959 *U. S. Patent* US3138743A
[3] Noyce R 1959 *U. S. Patent* US2981877A
[4] 2013 *International Technology Roadmap for Semiconductor (ITRS)* URL `http://www.itrs.net`
[5] Ishikawa Y and Saito S 2014 *IEICE Electronics Express* **11** 1–17
[6] Zimmermann H 2000 *Integrated Silicon Opto-electronics* (Springer)
[7] Pavesi L and Lockwood D J (eds) 2004 *Silicon Photonics* (Springer)
[8] Reed G T and Knights A P 2004 *Silicon Photonics* (Wiley)
[9] Pavesi L and Guillot G (eds) 2006 *Optical Interconnects The Silicon Approach* (Springer)
[10] Reed G 2008 *Silicon Photonics the state of the art* (Wiley)
[11] Miller D A B 2009 *Proceedings of the IEEE* **97** 1166–1185
[12] Deen M J and Basu P K 2012 *Silicon Photonics Fundamentals and Devices* (Wiley)
[13] Fathpour S and Jalali B (eds) 2012 *Silicon Photonics for telecommunications and biomedicine* (CRC Press)
[14] Vivien L and Pavesi L (eds) 2013 *Handbook of Silicon Photonics* (Taylor and Francis)
[15] Arakawa Y, Nakamura T and Urino Y 2013 *Communications Magazine, IEEE* **51** 72–77
[16] Urino Y, Horikawa T, Nakamura T and Arakawa Y 2013 OM2J
[17] Lee A, Liu H and Seeds A 2013 *Semicond Sci. Technol.* **28** 015027
[18] Gunn C 2006 *Micro, IEEE* **26** 58–66
[19] Fang A W, Park H, Cohen O, Jones R, Paniccia M J and Bowers J E 2006 *Opt. Express* **14** 9203–9210
[20] Liang D and Bowers J E 2010 *Nature Photonics* **4** 511–517
[21] Steger M, Yang A, Sekiguchi T, Saeedi K, Thewalt M L W, Henry M O, Johnston K, Riemann H, Abrosimov N V, Churbanov M F, Gusev A V, Kaliteevskii A K, Godisov O N, Becker P and Pohl H J 2011 *J. Appl. Phys.* **110** 081301
[22] Corbett B, Bower C, Fecioru A, Mooney M, Gubbins M and Justice J 2013 *Semicond Sci. Technol.* **28** 094001
[23] Smit M, Leijtens X, Ambrosius H, Bente E, van der Tol J, Smalbrugge B, de Vries T, Geluk E J, Bolk J, van Veldhoven R, Augustin L, Thijs P, D'Agostino D, Rabbani H, Lawniczuk K, Stopinski S, Tahvili S, Corradi A, Kleijn E, Dzibrou D, Felicetti M, Bitincka E, Moskalenko V, Zhao J, Santos R, Gilardi G, Yao W, Williams K, Stabile P, Kuindersma P, Pello J, Bhat S, Jiao Y, Heiss D, Roelkens G, , Wale M, Firth P, Soares F, Grote N, Schell M, Debregeas H, Achouche M, Gentner J L, Bakker A, Korthorst T, Gallagher D, Dabbs A, Melloni A, Morichetti F, Melati D, Wonfor A, Penty R, Broeke R, Musk B and Robbins D 2014 *Semicond Sci. Technol.* **29** 083001
[24] Sun X, Liu J, Kimerling L C and Michel J 2010 *IEEE J. Selec. Top. Quant. Elec.* **16** 124–131
[25] Liu J, Camacho-Aguilera R, Bessette J T, Sun X, Wang X, Cai Y, Kimerling L C and Michel J 2012 *Thin Solid Films* **520** 3354–3360
[26] Michel J and Romagnoli M 2012 *SPIE*
[27] Bolkhovityanov Y B and Sokolov L V 2012 *Semicond Sci. Technol.* **27** 043001
[28] Boucaud P, Kurdi M E, Ghrib A, Prost M, de Kersauson M, Sauvage S, Aniel F, Checoury X, Beaudoin G, Largeau L, Sagnes I, Ndong G, Chaigneau M and Ossikovski R 2013 *Photon. Res.* **1** 102–109
[29] Liu J 2014 *Photonics* **1** 162–197
[30] Saito S, Gardes F Y, Al-Attili A Z, Tani K, Oda K, Suwa Y, Ido T, Ishikawa Y, Kako S, Iwamoto S and Arakawa Y 2014 *Front. Mat.* **1** 15
[31] Geiger R, Zabel T and Sigg H 2015 *Front. Mat.* **2** 52
[32] Canham L T 1990 *Appl. Phys. Lett.* **57** 1046–1048
[33] Koshida N and Koyama H 1992 *Appl. Phys. Lett.* **60** 347–349
[34] Cullis A G, Canham L T and Calcott P D J 1997 *J. Appl. Phys.* **82** 909–965

[35] Gelloz B and Koshida N 2000 *J. Appl. Phys.* **88** 4319–4324

[36] Nassiopoulou A G 2004 *Silicon Nanocrystals in $SiO_2$ Thin Layers* vol 9 (American Scientific Publishers) pp 793–813

[37] Ossicini S, Pavesi L and Priolo F 2003 *Light Emitting Silicon for Microphotonics* (Springer)

[38] Gelloz B, Kojima A and Koshida N 2005 *Appl. Phys. Lett.* **87** 031107

[39] Daldosso N and Pavesi L 2009 *Laser & Photon. Rev.* **3** 508–534

[40] Shakoor A, Savio R L, Cardile P, Portalupi S L, Gerace D, Welna K, Boninelli S, Franzò G, Priolo F, Krauss T F, Galli M and O'Faolain L 2013 *Laser & Photon. Rev.* **7** 114–121

[41] Newman R 1953 *Phys. Rev.* **91** 1313–1314

[42] Haynes J R 1955 *Phys. Rev.* **98** 1866–1868

[43] Zhang Q, Huang J, Wu N, Chen G, Hong M, Bera L K and Zhu C 2006 *IEEE Electron Device Lett.* **27** 728–730

[44] Feng J, Woo R, Chen S, Liu Y, Griffin P B and Plummer J D 2007 *IEEE Electron Device Lett.* **28** 637–639

[45] Feng J, Thareja G, Kobayashi M, Chen S, Poon A, Bai Y, Griffin P B, Wong S S, Nishi Y and Plummer J D 2008 *IEEE Electron Device Lett.* **29** 805–807

[46] Luan H C, Lim D R, Lee K K, Chen K M, Sandland J G, Wada K and Kimerling L C 1999 *Appl. Phys. Lett.* **75** 2909

[47] Ishikawa Y, Wada K, Cannon D D, Liu J, Luan H C and Kimerling L C 2003 *Appl. Phys. Lett.* **82**

[48] Liu J, Sun X, Kimerling L C and Michel J 2009 *Opt. Lett.* **34** 1738–1740

[49] Cheng T H, Kuo P S, Lee C T, Liao M, Hung T A and Liu C W 2007 Electrically pumped Ge laser at room temperature *IEEE Int. Conf. Electron Devices Meeting (IEDM)* pp 659–662

[50] Camacho-Aguilera R E, Cai Y, Patel N, Bessette J T, Romagnoli M, Kimerling L C and Michel J 2012 *Opt. Express* **20** 11316–11320

[51] Koerner R, Oehme M, Gollhofer M, Schmid M, Kostecki K, Bechler S, Widmann D, Kasper E and Schulze J 2015 *Opt. Express* 14815–14822

[52] Andronov A A, Zverev I V, Kozlov V A, Nozdrin Y N, Pavlov S A and Shastin V N 1984 *JETP Lett.* **40** 804–807

[53] Komiyama S, Iizuka N and Akasaka Y 1985 *Appl. Phys. Lett.* **47** 958–960

[54] Hübers H W, Pavlov S G and Shastin V N 2005 *Semicond Sci. Technol.* **20** S221

[55] Wirths S, Geiger R, von den Driesch N, Mussler G, Stoica T, Mantl S, Ikonic Z, Luysberg M, Chiussi S, Hartmann J M, Sigg H, Faist J, Buca D and Grützmacher D 2015 *Nature Photo.* **9** 88–92

[56] Soref R A and Perry C H 1991 *J. Appl. Phys.* **69** 539–541

[57] Soref R A and Friedman L 1993 *Superlattices and Microstructures* **14** 189–193

[58] Soref R 2010 *Nature Photo.* **4** 495–497

[59] Boztug C, Sánchez-Pérez J R, Cavallo F, Lagally M G and Paiella R 2014 *ACS NANO* **8** 3136–3151

[60] Yariv A and Yeh P 2006 *Photonics: Optical Electronics in Modern Communications* (Oxford University Press)

[61] Chuang S L 2009 *Physics of Photonic Devices* (Wiley)

[62] Hu W, Cheng B, Xue C, Xue H, Su S, Bai A, Luo L, Yu Y and Wang Q 2009 *Appl. Phys. Lett.* **95** 092102

[63] Sun X, Liu J, Kimerling L C and Michel J 2009 *Appl. Phys. Lett.* **95** 011911

[64] Sun X, Liu J, Kimerling L C and Michel J 2009 *Opt. Lett.* **34** 1198–1200

[65] Liu J, Sun X, Camacho-Aguilera R, Kimerling L C and Michel J 2010 *Optics Lett.* **35** 679–681

[66] Nishida K, Xu X, Sawano K, Maruizumi T and Shiraki Y 2014 *Thin Solid Films* **557** 66–69

[67] Xu X, Nishida K, Sawano K, Maruizumi T and Shiraki Y 2014 Resonant photoluminescence from ge microdisks on ge-on-insulator *7th Int. Conf. Silicon-Germanium Technology and Device Meeting (ISTDM)* pp 135–136

[68] Xu X, Nishida K, Sawano K, Maruizumi T and Shiraki Y 2014 Tensile-strained, heavily n-doped germanium-on-insulator for light emitting devices on silicon *Conf. Lasers and Electro-Optics (CLEO)* p SM4H.3

[69] Xu X, Wang X, Nishida K, Takabayashi K, Sawano K, Shiraki Y, Li H, Liu J and Maruizumi T 2015 *Appl. Phys. Express* **8** 092101

[70] Hartmann J M, Damlencourt J F, Bogumilowicz Y, Holliger P, Rolland G and Billon T 2005 *J. Crystal Growth* **274** 90–99

[71] Cheng S L, Lu J, Shambat G, Yu H Y, Saraswat K, Vučković J and Nishi Y 2009 *Opt. Express* **17** 10019–10024

[72] Hartmann J M, Barnes J P, Veillerot M, Fedeli J M, Benoit Q, Guillaume A L and Calvo V 2012 *J. Crystal Growth* **347** 37–44

[73] Shah V A, Dobbie A, Myronov M and Leadley D R 2011 *Thin Solid Films* **519** 7911–7917

[74] Rhead S D, Halpin J E, Shah V A, Myronov M, Patchett D H, Allred P S, Kachkanov V, Dolbnya I P, Reparaz J S, adn C M S Torres N R W and Leadley D R 2014 *Appl. Phys. Lett.* **104** 172107

[75] Isella G, Chrastina D, Rössner B, Hackbarth T, Herzog H J, König U and von Känel H 2004 *Solid State Electron.* **48** 1317–1323

[76] Osmond J, Isella G, Chrastina D, Kaufmann R, Acciarri M and von Känel H 2009 *Appl. Phys. Lett.* **94** 201106

[77] Carroll L, Friedli P, Neunschwander S, Sigg H, Cecchi S, Isa F, Chrastina D, Isella G, Fedoryshyn Y and Faist J 2012 *Phys. Rev. Lett.* **109**

[78] Süess M J, Geiger R, Minamisawa R A, Schiefler G, J Frigerio D C, Isella G, Spolenak R, Faist J and Sigg H 2013 *Nature Photonics* **7** 466–472

[79] Arakawa Y and Sakaki H 1982 *Appl. Phys. Lett.* **40** 939–941

[80] Cai Y, Han Z, Wang X, Camacho-Aguilera R, Kimerling L C, Michel J and Liu J 2013 *J. Sel. Top. Quant. Electron.* **19** 1901009

[81] Menéndez J and Kouvetakis J 2004 *Appl. Phys. Lett.* **85** 1175

[82] Saito S, Takahama T, Tani K, Takahashi M, Mine T, Suwa Y and Hisamoto D 2011 *Appl. Phys. Lett.* **98** 261104

[83] Saito S, Oda K, Takahama T, Tani K and Mine T 2011 *Appl. Phys. Lett.* **99** 241105

[84] Tani K, Saito S, Oda K, Miura M, Mine T, Sugawara T and Ido T 2011 Ge(111)-fin light-emitting diodes *IEEE 8th Int. Conf. Group IV Photonics* pp 217–219

[85] Hisamoto D, Lee W, Kedzierski J, Takeuchi H, Asano K, Kuo C, Anderson E, King T, Bokor J and Hu C 2000 *IEEE Trans. Electron Devices* **47** 2320–2325

[86] Liu J, Sun X, Pan D, Wang X, Kimerling L C, Koch T L and Michel J 2007 *Opt. Express* **15** 11272–11277

[87] Suwa Y and Saito S 2010 First-principles study of light emisson from germanium guantum-well *IEEE 22nd Int. Semiconductor Laser Conference (ISLC)* pp 131–132

[88] Suwa Y and Saito S 2011 First-principles study of light emission from silicon and germanium due to direct tranistions *IEEE 8th Int. Conf. Group IV Photonics* pp 222–224

[89] Virgilio M, Manganelli C L, Grosso G, t Schroeder and Capellini G 2013 *J. Appl. Phys.* **114**

[90] Virgilio M, Manganelli C L, Grosso G, Pizzi G and Capellini G 2013 *Phys. Rev. B* **87** 235313

[91] Liu Z, Li Y, He C, Li C, Xue C, Zuo Y, Cheng B and Wang Q 2014 *Appl. Phys. Lett.* **104** 191111

[92] Al-Attili A Z, Kako S, Husain M K, Gardes F Y, Arimoto H, Higashitarumizu N, Iwamoto S, Arakawa Y, Ishikawa Y and Saito S 2015 *Jpn. J. Appl. Phys.*

[93] Giovane L M, Luan H C, Agarwal A M and Kimerling L C 2001 *Applied Physics Letters* **78** 541 ISSN 00036951 URL `http://link.aip.org/link/APPLAB/v78/i4/p541/s1&Agg=doi`

[94] Gaubas E and Vanhellemont J 2006 *Applied Physics Letters* **89** 142106 ISSN 00036951 URL `http://link.aip.org/link/APPLAB/v89/i14/p142106/s1&Agg=doi`

[95] Kako S, Okumura T, Oda K, Suwa Y, Saito S, Ido T and Arakawa Y 2012 *The 9th International Conference on Group IV Photonics (GFP)* **7** 340–342 URL `http://ieeexplore.ieee.org/lpdocs/epic03/wrapper.htm?arnumber=6324180`

[96] Sheng J J, Leonhardt D, Han S M, Johnston S W, Cederberg J G and Carroll M S 2013 *Journal of Vacuum Science & Technology B: Microelectronics and Nanometer Structures* **31** 051201 ISSN 21662746 URL http://scitation.aip.org/content/avs/journal/jvstb/31/5/10.1116/1.4816488

[97] Geiger R, Frigerio J, Süess M J, Chrastina D, Isella G, Spolenak R, Faist J and Sigg H 2014 *Applied Physics Letters* **104** 062106 ISSN 0003-6951 URL http://scitation.aip.org/content/aip/journal/apl/104/6/10.1063/1.4865237

[98] de Walle C G V and Martin R M 1986 *Phys. Rev. B* **34** 5621–5634

[99] de Walle C G V 1989 *Phys. Rev. B* **39** 1871

[100] Ortolland C, Okuno Y, Veheyen P, Kerner C, Stapelmann C, Aoulaiche M, Horiguchi N and Hoffmann T 2009 *Electron Devices, IEEE Transactions on* **56** 1690–1697

[101] Tani K, Oda K, Okumura T, Takezaki T, Kasai J, Mine T and Ido T 2013 Enhanced electroluminescence from germanium waveguides by local tensile strain with silicon nitride stressors *International Conference on Solid State Devices and Materials (SSDM)* (Fukuoka) pp K–6–3

[102] Oda K, Okumura T, Tani K, Saito S and Ido T 2014 *Thin Solid Films* **557** 355–362

[103] Lim P H, Park S, Ishikawa Y and Wada K 2009 *Opt. Express* **17** 16358–16365

[104] Nam D, Sukhdeo D, Roy A, Balram K, Cheng S L, Huang K C Y, Yuan Z, Brongersma M, Nishi Y, Miller D and Saraswat K 2011 *Opt. Express* **19** 25866–25872

[105] Jain J R, D S Ly-Gagnon K C B, White J S, Brongersma M L, Miller D A B and Howe R T 2011 *Opt. Mat. Express* **1** 1121–1126

[106] Jain J R, Hryciw A, Baer T M, Miller D A B, Brongersma M L and Howe R T 2012 *Nature Photonics* **6** 398–405

[107] Tani K, Saito S, Lee Y, Oda K, Mine T, Sugawara T and Ido T 2012 *Jpn. J. Appl. Phys.* **51** 04DG09

[108] Klesse W M, Scappucci G, Capellini G, Hartmann J M and Simmons M Y 2013 *Appl. Phys. Lett.* **102** 151103

[109] Moriya Y, Ikeda K, Takeuchi S, Kamimuta Y, Nakamura Y, Izunome K, Sakai A and Tezuka T 2014 *Appl. Phys. Express* **7** 086501

[110] Petykiewicz J, Nam D, Sukhdeo D S, Gupta S, Buckley S, Piggott A Y, Vučković J and Saraswat K C 2015 *arXiv* 1508.01255v1

[111] Hashimoto T, Yoshimoto C, Hosoi T, Shimura T and Watanabe H 2009 *Appl. Phys. Express* **2** 066502

[112] Miyao M, Tanaka T, Toko K and Tanaka M 2009 *Appl. Phys. Express* **2** 045503

[113] Tang S H, Chang D Y, Hudait M, Maa J S, Liu C W, Luo G L, Trinh H D and Su Y H 2011 *Appl. Phys. Lett.* **98** 161905

[114] Ghrib A, de Kersauson M, Kurdi M E, Jakomin R, Beaudoin G, Sauvage S, Fishman G, Ndong G, Chaigneau M, Ossikovski R, Sagnes I and Boucaud P 2012 *Appl. Phys. Lett.* **100** 201104

[115] Ghrib A, Kurdi M E, de Kersauson M, Prost M, Sauvage S, Checoury X, Beaudoin G, Sagnes I and Boucaud P 2013 *Appl. Phys. Lett.* **102** 221112

[116] Hoshina Y, Yamada A and Konagai M 2009 *Jpn. J. Appl. Phys.* 111102

[117] Huo Y, Lin H, Chen R, Makarova M, Rong Y, Li M, Kamins T I, Vučković J and Harris J S 2011 *Appl. Phys. Lett.* **98** 011111

[118] Nam D, Sukhdeo D, Cheng S L, Roy A, Huang K C Y, Brongersma M, Nishi Y and Saraswat K 2012 *Appl. Phys. Lett.* **100** 131112

[119] Tseng C K, Chen W T, Chen K H, Liu H D, Kang Y, Na N and Lee M C M 2013 *Scientific Reports* **3** 3225

[120] Nakaharai S, Tezuka T, Sugiyama N, Moriyama Y and Takagi S 2003 *Appl. Phys. Lett.* **83** 3516–3518

[121] Nakaharai S, Tezuka T, Hirashita N, Toyoda E, Moriyama Y, Sugiyama N and Takagi S 2007 *Semicond Sci. Technol.* **22** S103–S106

[122] Nakaharai S, Tezuka T, Hirashita N, Toyoda E, Moriyama Y, Sugiyama N and Takagi S 2009 *J. Appl. Phys.* **105** 024515
[123] Tezuka T, Toyoda E, Irisawa T, Hirashita N, Moriyama Y, Sugiyama N, Usuda K and Takagi S 2009 *Appl. Phys. Lett.* **94** 081910
[124] Dissanayake S, Shuto Y, Sugahara S, Takenaka M and Takagi S 2008 *Thin Solid Films* **517** 178–180
[125] Oda K, Tani K, Saito S i and Ido T 2014 *Thin Solid Films* **550** 509–514
[126] Nayfeh A, Chui C O and Saraswat K C 2004 *Appl. Phys. Lett.* **85** 2815
[127] Mukherjee C, Seitz H and Schröder B 2001 *Appl. Phys. Lett.* **78** 3457–3459
[128] Gity F, Daly A, Snyder B, Peters F H, Hayes J, Colinge C, Morrison A P and Corbett B 2013 *Opt. Express* **21** 17309–17314
[129] Ngo T P, Kurdi M E, Checoury X, Boucaud P, Damlencourt J F, Kermarrec O and Bensahel D 2008 *Appl. Phys. Lett.* **93** 241112
[130] Oda K, Tani K, Saito S and Ido T 2012 *ECS Transactions* **50** 277–286
[131] Kozlowski G, Yamamoto Y, Bauer J, Schubert M A, Dietrich B, Tillack B and Schroeder T 2011 *J. Appl. Phys.* **110** 05309
[132] Cheng T H, Ko C Y, Chen C Y, Peng K L, Luo G L, Liu C W and Tseng H H 2010 *Appl. Phys. Lett.* **96** 091105
[133] d Kersauson M, Jakomin R, Kurdi M E, Beaudoin G, Zerounian N, Aniel F, Sauvage S, Sagnes I and Boucaud P 2010 *J. Appl. Phys.* **108** 023105
[134] Liu Y, Deal M D and Plummer J D 2004 *Appl. Phys. Lett.* **84** 2563
[135] Hu S, Marshall A F and Mclntyre P C 2010 *Appl. Phys. Lett.* **97** 082104
[136] Lee E K, Lockwood D J, Baribeau J M, Brakovsky A M, Kamins T I and Tsybeskov L 2009 *Phys. Rev. B* 233307
[137] Lange C, Köster N S, Chatterjee S, Sigg H, Chrastina D, Isella G, von Känel H, Süess M, Kira M and Koch S W 2009 *Phys. Rev. B* **79** 201306(R)
[138] Carroll L, Imbert F, Sigg H, Süess M, MSüller E, Virgilio M, Pizzi G, Rossbach P, Chrastina D and Isella G 2011 *Appl. Phys. Lett.* 031907
[139] Chen Y, Li C, Zhou Z, Lai H, Chen S, Ding W, Cheng B and Yu Y 2009 *Appl. Phys. Lett.* **94** 141902
[140] Zhou Z, Li C, Lai H, Chen S and Yu J 2008 *J. Crystal Growth* **310** 2508–2513
[141] Ortolani M, Stehr D, Wagner M, Helm M, Pizzi G, Virgilio M, Grosso G, Capellini G and Seta M D 2011 *Appl. Phys. Lett.* **99** 201101
[142] Ren S, Rong Y, Kamins T I, Harris J S and Miller D A B 2011 *Appl. Phys. Lett.* **98** 151108
[143] Nguyen Q T, Damlencourt J F, Vincent B, Clavelier L, Morand Y, Gentil P and Cristoloveanu S 2007 *Solid State Electron.* **51** 1172–1179
[144] Fukatsu S, Usami N, Chinzei T, Shiraki Y, Nishida A and Nakagawa K 1992 *Jpn. J. Appl. Phys.* **31** L1015–L1017
[145] Boztug C, Sanchez-Perez J R, Yin J, Lagally M G and Paiella R 2013 *Appl. Phys. Lett.* **103** 201114
[146] Kamenev B V, Tsybeskov L, Baribeau J M and Lockwood D J 2004 *Appl. Phys. Lett.* **84** 1293–1295
[147] Nataraj L, Xu F and Cloutier S G 2010 *Opt. Express* **18** 7085–7091
[148] Zhong Z, Halilovic A, Mühlberger M, Schäffler F and Bauer G 2003 *J. Appl. Phys.* **93** 6258–6264
[149] Borgström M, Zela V and Seifert W 2003 *Nanotechnology* **14** 264–267
[150] Shklyaev A A and Ichikawa M 2008 *Physics-Uspekhi* **51** 133–161
[151] Hauke N, Lichtmannecker S, Zabel T, Laussy F P, Laucht A, Kaniber M, Bougeard D, Abstreiter G, Finley J J and Arakawa Y 2011 *Phys. Rev. B* **84** 085320
[152] Hauke N, Tandaechanurat A, Zabel T, Reichert T, Takagi H, Kaniber M, Iwamoto S, Bougeard D, Finley J J, Abstreiter G and Arakawa Y 2012 *New J. Phys.*
[153] Zhang Y, Zeng C, Li D, Zhao X, Gao G, Yu J and Xia J 2014 *Opt. Express* **22** 12248–12254

[154] Bauer M, Ritter C, Crozier P A, Ren J, Menendez J, Wolf G and Kouvetakis J 2003 *Appl. Phys. Lett.* **83** 2163–2165
[155] D'Costa V R, Cook C S, Birdwell A G, Littler C L, Canonico M, Zollner S, Kouvetakis J and Menédez J 2006 *Phys. Rev. B* **73** 125207
[156] Tseng H H, Wu K Y, Li H, Mashanov V, Cheng H H, Sun G and Sorel R A 2013 *Appl. Phys. Lett.* **102** 182106
[157] Fang Y Y, Tolle J, Roucka R, Chizmeshya A V G, Kouvetakis J, D'Costa V R and Menédez J 2007 *Appl. Phys. Lett.* **90** 061915
[158] Matthews J W, Mader S and Light T B 1970 *J. Appl. Phys.* **41** 3800–3804
[159] People R 1986 *IEEE J. Selec. Top. Quant. Elec.* **22**
[160] Kimura Y, Sugii N, Kimura S, Inui K and Hirasawa W 2006 *Appl. Phys. Lett.* **88** 031912
[161] Ootsuka F, Wakahara S, Ichinose K, Honzawa A, Wada S, Sato H, Ando T, Ohta H, Watanabe K and Onai T 2000 A highly dense, high-performance 130 nm node cmos technology for large scale system-on-a-chip applications *IEEE Int. Conf. Electron Devices Meeting (IEDM)* pp 575–578
[162] Shimizu A, Hachimine K, Ohki N, Ohta H, Koguchi M, Nonaka Y, Sato H and Ootsuka F 2001 Local mechanical-stress control (lmc): a new technique for cmos-performance enhancement *IEEE Int. Conf. Electron Devices Meeting (IEDM)* pp 19.4.1–19.4.4
[163] Bruel M 1994 *U. S. Patent* US5374564A
[164] Ishikawa Y, Wada K, Liu J, Cannon D D, Luan H C, Michel J and Kimerling L C 2005 *J. Appl. Phys.* **98** 013501
[165] Ishikawa Y and Wada K 2010 *Thin Solid Films* **518** S83–S87
[166] Camacho-Aguilera R, Han Z, Cai Y, Kimerling L C and Michel J 2013 *Appl. Phys. Lett.* **102** 152106
[167] Sánchez-Pérez J R, Boztug C, Chen F, Sudradjat F F, Paskiewicz D M, Jacobson R B, Lagally M G and Paiella R 2011 Direct-bandgap light-emitting gremanium in tensilely strained nanomembranes *Proceedings of the National Academy of Sciences of USA (PNAS)* vol 108 pp 18893–18898
[168] de Kersauson M, Kurdi M E, David S, Checoury X, Fishman G, Sauvage S, Jakomin R, Beaudoin G, Sagnes I and Boucaud P 2011 *Opt. Express* **19** 17925–17934
[169] Capellini G, Kozlowski G, Yamamoto Y, Lisker M, Wenger C, Niu G, Zaumseil P, Tillack B, Ghib A, d Kersauson M, Kurdi M E, Boucaud P and Schroeder T 2013 *J. Appl. Phys.* **113** 013513
[170] Capellini G, Reich C, Guha S, Yamamoto Y, Lisker M, Virgilio M, Ghrib A, Kurdi M E, Boucaud P, Tillack B and Schroeder T 2014 *Opt. Express* **22** 399–410
[171] Kurdi M E, Bertin H, Martincic E, de Kersauson M, Fishman G, Sauvage S, Bosseboeuf A and Boucaud P 2010 *Appl. Phys. Lett.* **96** 041909
[172] Nama D, Sukhdeo D S, Kang J H, Petykiewicz J, Lee J H, Jung W S, Vučković J, Brongersma M L and Saraswat K C 2013 *Nano Lett.* **13** 3118–3123
[173] Sukhdeo D S, Nam D, Kang J H, Brongersma M L and Saraswat K C 2014 *Photon. Res.* **2** A8–A13
[174] Cerdeira F, Buchenauer C J, Pollak F H and Cardona M 1972 *Phys. Rev. B* **5** 580–593
[175] Peng C Y, Huang C F, Fu Y C, Yang Y H, Lai C Y, Chang S T and Liu C W 2009 *J. Appl. Phys.* **105** 083537
[176] Ghib A, Kurdi M E, Prost M, Sauvage S, Checoury X, Beaudoin G, Chaigneau M, Ossikovski R, Sagnes I and Boucaud P 2015 *Adv. Optical Mater.* **3** 353–358
[177] Al-Attili A Z, Kako S, Husain M K, Gardes F Y, Higashitarumizu N, Iwamoto S, Arakawa Y, Ishikawa Y, Arimoto H, Oda K, Ido T and Saito S 2015 *Front. Mat.* **2** 43
[178] Stoney G G 1909 The tension of metallic films deposited by electrolysis *Proc. R. Soc. London Ser. A* vol 82 pp 172–175
[179] Janssen G C A M, Abdalla M M, v Keulen F, Pujada R P and v Venrooy B 2009 *Thin Solid Films* **517** 1858–1867

[180] Cheng S L, Shambat G, Lu J, Yu H Y, Saraswat K, Kamins T I, Vučković J and Nishi Y 2011 *Appl. Phys. Lett.* **98** 211101

[181] Scappucci G, Capellini G, Klesse W M and Simmons M Y 2011 *Nanotechnology* **22** 375203

[182] Kurdi M E, Kociniewski T, Ngo T P, Boulmer J, ad P Boucaud D D, Damlencourt J F, Kermarrec O and Bensahel D 2009 *Appl. Phys. Lett.*

[183] Sawano K, Hoshi Y, Kasahara K, Yamane K, Hamaya K, Miyao M and Shiraki Y 2010 *Appl. Phys. Lett.* **97** 162108

[184] Yurasov D V, Antonov A V, Drozdov M N, Schmagin V B, Spirin K E and Novikov A V 2015 *J. Appl. Phys.* **118** 145701

[185] Ioannou N, Skarlatos D, Tsamis C, Krontiras C A, Georga S N, Christofi A and McPhail D S 2008 *Appl. Phys. Lett.* **93** 101910

[186] Park J H, Kuzum D, Tada M and Saraswat K C 2008 *Appl. Phys. Lett.* **93** 193507

[187] Chen W B, Shie B S, Chin A, Hsu K C and Chi C C 2010 High-k metal-gate/high-k/ge n-mosfets with $<$ 1 nm eot using laser annealing *IEEE Int. Conf. Electron Devices Meeting (IEDM)* p 18.2.1

[188] Wündisch, Posselt M, Schmidt B, Heera V, Schumann T, Mücklich A, Grötzschel R, Skorupa W, Clarysse T, Simoen E and Hortenbach H 2009 *Appl. Phys. Lett.* **95** 252107

[189] Kim J, Bedell S W, Maurer S L, Loesing R and Sadana D K 2010 *Electro. Solid-State Lett.* **13** H12–H15

[190] Takenaka M, Morii K, Sugiyama M, Nakano Y and Takagi S 2012 *Opt. Express*

[191] Cammilleri D, F Fossard D D, Manh C T, Dubois C, Bustarret E, Marcenat C, Achatz P, Bouchier D and Boulmer J 2008 *Thin Solid Films* 75–79

[192] Posthuma N E, v d Heide J, Flamand G and Poortmans J 2007 *IEEE Trans. Electron Devices* **54** 1210–1215

[193] Michel J, Liu J and Kimerling L C 2010 *Nature Photonics* **4** 527–534

[194] Sze S M and Lee M K 2012 *Semiconductor Devices: Physics and Technology* 3rd ed (John Wiley and Sons)

[195] Taur Y and Ning T H 2013 *Fundamentals of Modern VLSI Devices* 2nd ed (Cambridge University Press)

[196] Jannopoulos J D and Winn R D M J N 1995 *Photonic Crystals* (Princeton: Princeton University Press)

[197] Lim P H, Kobayashi Y, Takita S, Ishikawa Y and Wada K 2008 *Appl. Phys. Lett.* **93** 041103

[198] Xia J S, Nemoto K, Ikegami Y, Shiraki Y and Usami N 2007 *Appl. Phys. Lett.* **91** 011104

[199] Xia J, Takeda Y, Usami N, Maruizumi T and Shiraki Y 2010 *Opt. Express* **18** 13945–13950

[200] Shambat G, Cheng S L, Lu J, Nishi Y and Vučković J 2010 *Appl. Phys. Lett.* **97** 241102

[201] David S, Kurdi M E, Boucaud P, Chelnokov A, Thanh V L, Bouchier D and Lourtioz J M 2003 *Appl. Phys. Lett.* **83** 2509–2511

[202] Xia J S, Ikegami Y, Shiraki Y, Usami N and Nakata Y 2006 *Appl. Phys. Lett.* **89** 201102

[203] Xia J, Tominaga R, Fukamitsu S, Usami N and Shiraki Y 2009 *Jpn. J. Appl. Phys.* **48** 022102

[204] Kurdi M E, Checoury X, David S, Ngo T P, Zerounian N, Boucaud P, Kermarrec O, Campidelli Y and Bensahel D 2008 *Opt. Express* **16** 8780–8791

[205] Iwamoto S, Arakawa Y and Gomyo A 2007 *Appl. Phys. Lett.* **91** 211104

[206] Nakayama S, Iwamoto S, Ishida S and Arakawa Y 2010 Demonstration of a silicon photonic crystal slab led with efficient electroluminescence *International Conference on Solid State Devices and Materials (SSDM)* pp D–4–3

[207] Nakayama S, Iwamoto S, Ishida S, Bordel D, Augedre E, Calvelier L and Arakawa Y 2010 *Physica E* **42** 2556–2559

[208] Nakayama S, Ishida S, Iwamoto S and Arakawa Y 2012 *Appl. Phys. Lett.* **98**

[209] Nakayama S, Iwamoto S, Kako S, Ishida S and Arakawa Y 2011 Demonstration of silicon nanocavity led with enhanced luminescence *International Conference on Solid State Devices and Materials* pp I–8–2

[210] Iwamoto S and Arakawa Y 2012 *IEICE Trans. Electron* **E95-C**
[211] Fujita M, Tanaka Y and Noda S 2008 *IEEE J. Selec. Top. Quant. Elec.* **14**
[212] Purcell E M 1946 *Phys. Rev* **69** 681
[213] Parker M A 2005 *Physics of Optoelectronics* (CRC Press Taylor & Francis Group)
[214] Coleman S 1985 *Aspects of Symmetry* (Cambridge University Press)